

# Linear Acceleration Is a Primary Risk Factor for Concussion

Jessica A. Towns<sup>1</sup>, Fady F. Abayazid<sup>2</sup>, James W. Hickey<sup>3</sup>, William T. O'Brien<sup>3</sup>, Spencer S.H. Roberts<sup>4</sup>, N. Stewart Pritchard<sup>5,6</sup>, Jillian E. Urban<sup>5,6</sup>, Joel D. Stitzel<sup>5,6</sup>, Gerald A. Grant<sup>7</sup>, Michael M. Zeineh<sup>8</sup>, Stuart J. McDonald<sup>3,9</sup>,  
David B. Camarillo<sup>1</sup>

<sup>1</sup>Department of Bioengineering, Stanford University, Stanford, CA

<sup>2</sup>Dyson School of Design Engineering, Imperial College London, London, UK

<sup>3</sup>Department of Neuroscience, School of Translational Medicine, Monash University, Melbourne, VIC

<sup>4</sup>Centre for Sport Research, Institute for Physical Activity and Nutrition, Deakin University, Geelong, Australia

<sup>5</sup>Center for Injury Biomechanics, Virginia Tech-Wake Forest University, Blacksburg, VA

<sup>6</sup>Wake Forest University School of Medicine, Winston-Salem, NC

<sup>7</sup>Department of Neurosurgery, Duke University, Durham, NC

<sup>8</sup>Department of Radiology, Stanford University, Stanford, CA

<sup>9</sup>Department of Neurology, Alfred Health, Melbourne, VIC

---

## Summary

Rotational acceleration of the head has long been posited as the primary cause of concussion due to its ability to generate shear strains that disrupt neuronal structure and function.<sup>1,2</sup> Linear acceleration, by contrast, is considered less injurious due to the brain's suspension in cerebrospinal fluid within the rigid skull.<sup>3,4</sup> As a result, the rotational acceleration hypothesis has predominantly driven international safety standards and protective equipment design. However, direct measurements of rotational acceleration during human concussion remain limited, leaving the rotational hypothesis largely untested *in vivo*. Here we show that linear acceleration is a significantly more precise predictor of concussion than rotational acceleration. We used mouthguards instrumented with inertial sensors to directly measure head kinematics during concussions occurring in children and adults of both sexes. Surprisingly, we found that rotational acceleration was not a significant independent predictor of concussion. Finite-element computed brain strains also had little predictive power, suggesting limitations in modeling the intracranial contents purely as solid materials. We suspect that modeling cerebrospinal fluid flow might reveal a protective effect that is limited by the magnitude of linear acceleration and the size of the subarachnoid space. Inspired by the protective role of cerebrospinal fluid, we invented a liquid shock absorbing technology and modeled it in a bicycle helmet. Using linear acceleration as a concussion risk function, we predict that our liquid technology can reduce the risk of concussion by up to 73% compared to a conventional foam helmet. Together, our findings support the inclusion of linear acceleration in concussion safety regulations and the need for advanced technologies to reduce impact forces and injury risk.

## Introduction

Traumatic brain injury (TBI) is a leading cause of death and disability worldwide and carries a global incidence of nearly 69 million cases per year.<sup>5</sup> Approximately 80-90% of TBIs are “mild” closed head injuries, or concussions,<sup>6</sup> but they can still result in neurodegenerative conditions such as chronic traumatic encephalopathy,<sup>7,8</sup> and prolonged psychological impairment such as post-traumatic stress disorder.<sup>9</sup> The biomechanical cause of closed-head TBI was first proposed during World War II, when A.H.S. Holbourn hypothesized that rotational acceleration of the head induces shear strains within brain tissue.<sup>10</sup> This concept later became the foundational hypothesis for diffuse, closed-head injury. The biophysical basis for the rotational acceleration hypothesis is that the massive human brain is a soft, gel-like structure that shears as it lags behind the rotating skull.<sup>11</sup> In contrast to rotational motion, linear acceleration transmits compressive forces to the head rather than shear. Because the brain and cerebrospinal fluid are nearly incompressible, compressive loading causes little deformation but can result in large pressures, where neurons have shown to be insensitive at pressures up to 540 Pa.<sup>12</sup> As a result, rotational kinematics and strain are the primary diffuse brain injury criteria for many safety standards.

Early support for the rotational hypothesis emerged from large animal models of moderate-to-severe TBI, and later shifted toward mild TBI, or concussion. During the 1960s and 70s, Ommaya and Gennarelli demonstrated that rotational loading could produce loss of consciousness and widespread axonal pathology in non-human primates.<sup>13–15</sup> Margulies and colleagues extended this work using porcine models, applying rotational accelerations to replicate milder injury patterns observed in human concussion.<sup>16</sup> Finite element (FE) models of the porcine brain have since shown that rotational acceleration induces diffuse strain particularly in the deep white matter,<sup>17</sup> a region heavily implicated by axonal pathology.<sup>18,19</sup> Together, these studies motivated the need for human concussion measurements to translate findings from animals and establish clinically relevant concussion thresholds.

With the minimization of mechanoelectrical systems, it became possible to measure head impact kinematics with wearable sensors on humans and move toward developing injury risk functions and tolerance thresholds for concussion. Injury risk functions estimate the probability of brain injury from mechanical inputs such as head motion or tissue deformation. Beginning in the early 2000s, the Head Impact Telemetry System (HITS)<sup>20</sup> enabled the first large-scale data collection studies in helmeted sports by embedding accelerometers into American football helmets. Since then, HITS data has informed the Brain Injury Criterion (BrIC), a rotational velocity-based metric and injury risk function<sup>21</sup> proposed by the National Highway Traffic Safety Administration for automotive crash testing, and the Summation of Tests for the Analysis of Risk (STAR) helmet rating system for many different sports.<sup>22</sup> HITS used

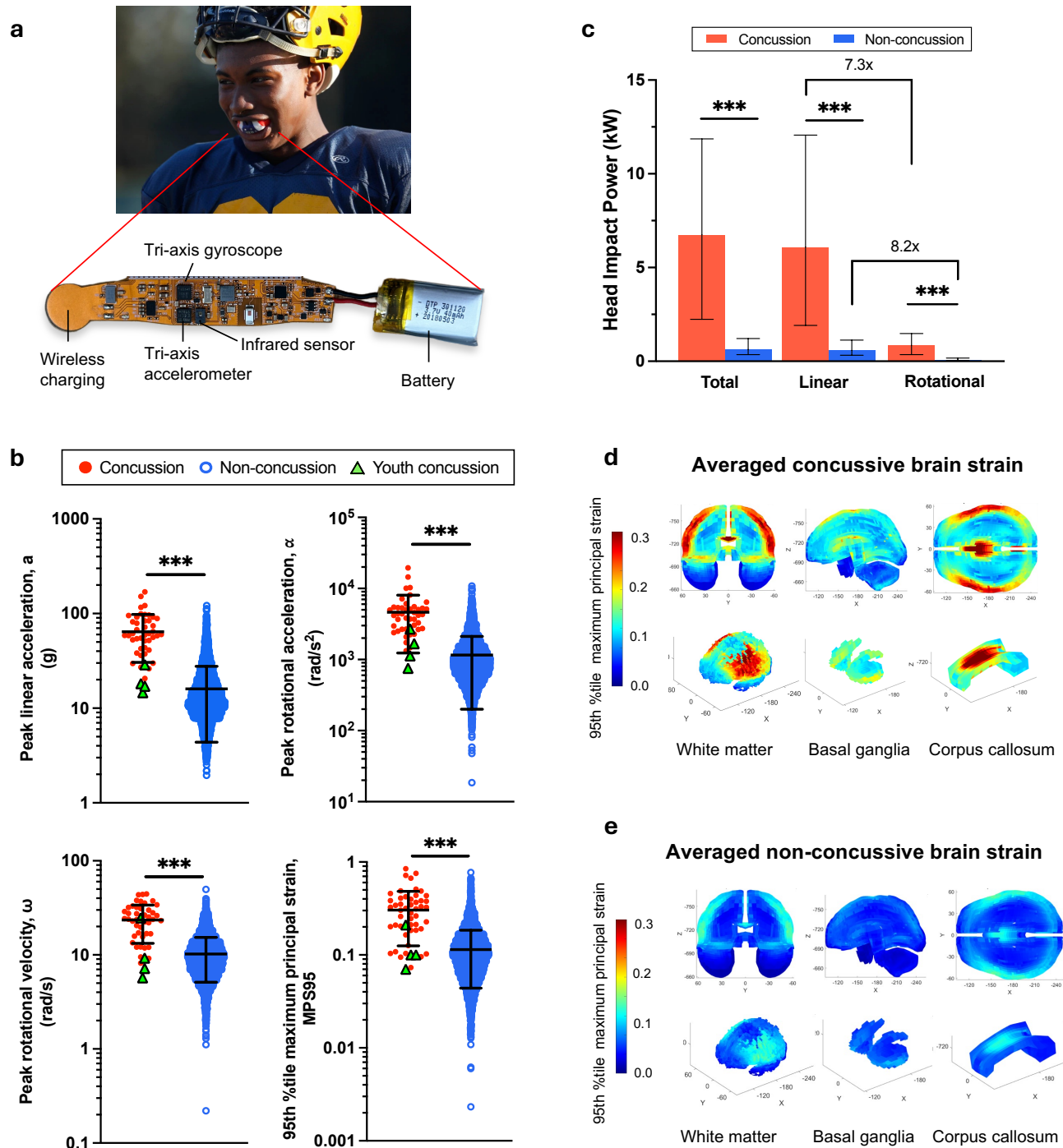
an array of helmet-mounted accelerometers to measure linear acceleration and estimated rotational acceleration using a centroid-based algorithm.<sup>23</sup> However, it did not capture time-resolved rotational acceleration and was affected by relative motion between the helmet and skull, reducing accuracy.<sup>23,24</sup>

Instrumented mouthguards (iMGs) overcome limitations of motion artifacts by rigidly coupling inertial sensors to the upper dentition, enabling direct six-degree-of-freedom measurements of linear and rotational head kinematics *in vivo*.<sup>25</sup> iMGs have been extensively tested in laboratory testing and on-field settings,<sup>26–28</sup> and deployed at scale in both helmeted and unhelmeted sports,<sup>29,30</sup> capturing large head impact datasets under real-world conditions. With these data now available, iMG technology offers the means to rigorously test the rotational hypothesis in humans and validate existing injury risk functions using *in vivo* measurements. By translating these findings into safety standards, the potential exists to substantially reduce the burden of concussion and other brain injuries in sectors such as industrial work safety, sports and recreation, transportation, military, and human-robot interaction, among many others. Here, we used a dataset of iMG-measured head impacts to test the hypothesis that rotational acceleration is a more precise predictor of concussion than linear acceleration, but we found the contrary. We also derived injury risk functions and found that injury thresholds for linear acceleration are much lower than current safety standards for concussion testing. We then developed a bio-inspired liquid cycling helmet that mimics the protective capabilities of cerebrospinal fluid against linear accelerations, and dramatically reduces estimated linear acceleration concussion risk compared to commercialized technology.

## Results

### Concussive impacts have larger kinematic and strain magnitudes

We characterized the kinematics and finite-element simulated strains from a dataset that included 3,805 non-concussive impacts and 47 concussive impacts, collected across 203 male and female athletes in American football, Australian football, rugby union, gymnastics, ice hockey, mixed martial arts (MMA) and lacrosse (Extended Data Table 1). Concussive impacts occurred in 40 athletes, with three American football players and one Australian football player sustaining multiple concussions. Loss of consciousness occurred in five Australian football cases, three MMA cases, one collegiate football case, and one youth football case. We calculated peak linear acceleration ( $a$ ), peak rotational acceleration ( $\alpha$ ), peak rotational velocity ( $\omega$ ), head impact power, split into linear and rotational components, and 95<sup>th</sup> percentile maximum principal strain (MPS95) both globally and regionally.



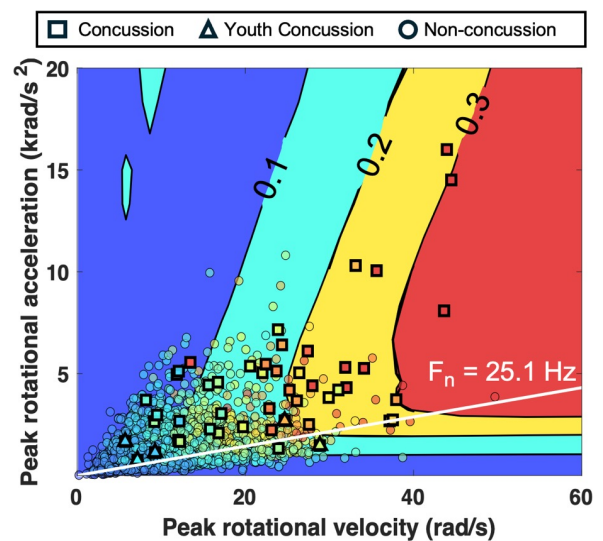
**Figure 1.** Differences in kinematics and brain strain between concussive and non-concussive impacts measured with instrumented mouthguards. **a**, Stanford MiG 2.0 and its sensor board components.<sup>31</sup> **b**, Distribution of impact magnitudes plotted on a logarithmic scale. Black bars represent the mean and one standard deviation of all impacts in each respective dataset. (\*\*\*,  $p < 0.0001$ ). **c**, Bar charts comparing head impact power for concussive and non-concussive impacts, split into linear and rotational components. Error bars indicate the interquartile range. In concussive impacts, the mean linear power was 7.3 times greater than the rotational power, while in non-concussive impacts, mean linear power was 8.2 times greater than the rotational power. Ninety-fifth percentile maximum principal strain patterns averaged across **d**, concussive and **e**, non-concussive impacts.

Figure 1a shows the Stanford MiG2.0, one of the iMG technologies used in this study, and its microelectronic sensor board components for measuring linear and rotational head impact forces. Figure 1b shows that concussive impacts exhibit significantly greater  $a$ ,  $\alpha$ ,  $\omega$ , and MPS95 compared to non-concussive impacts (\*\* $p < 0.0001$ ), and that youth concussion magnitudes are much lower than concussion data from older athletes for  $a$  and  $\alpha$ . Summary statistics of impact magnitudes are provided in Extended Data Table 2.

In Figure 1c, we plot differences in head impact power, the rate of change of kinetic energy of the head during an acceleration event, split into linear and rotational components. We found that on average, concussive impacts exhibited 7.3 times more linear power than rotational power, while non-concussive impacts had 8.2 times more linear than rotational power. This indicates that linear power, and by extension linear acceleration and velocity, are prominent biomechanical signatures of head impacts in our population.

In Figures 1d and 1e, we show differences in brain strain patterns for concussive and non-concussive impacts. Specifically, we show the MPS95 per element averaged across impact types. In concussive impacts, elevated strains are observed in the cortical areas including the upper gray matter ( $0.36 \pm 0.21$ ) and cortical white matter ( $0.30 \pm 0.12$ ), as well as the deep white matter regions such as the basal ganglia ( $0.28 \pm 0.10$ ) and corpus callosum ( $0.48 \pm 0.14$ ). Non-concussive impacts had significantly lower MPS95, ranging from 0.04 to 0.09. (Extended Data Table 3). These findings support Holbourn's original hypothesis that shear deformation underlies brain injury.

Figure 2 shows that the majority of impacts fall within a regime where brain deformation is expected to be more sensitive to rotational velocity than to rotational acceleration. This pattern is shown relative to the white reference line, which has a slope equal to the inverse of the brain's natural period,  $\Delta t_n$ , approximately 40.5 ms when averaged across coronal, sagittal, and axial anatomical planes.<sup>32</sup> This period corresponds to a natural frequency of approximately 25.1 Hz and represents the duration of one full oscillation of the brain when subjected to dynamic loading. Impacts above this line are indicative of short-duration pulses relative to the brain's natural period, where deformation is primarily influenced by rotational velocity. In this regime, peak rotational



**Figure 2.** Iso-strain contour plot showing the relationship between peak rotational velocity, peak rotational acceleration, and strain, as predicted by the DAMAGE model.<sup>12</sup> A white reference line is plotted with a slope defined as  $\pi/\Delta t_n$ , reflecting the brain's estimated natural frequency of 25.1 Hz.

velocity is reached before significant deformation accumulates. Conversely, impacts below the line are indicative of longer-duration pulses, where sustained rotational acceleration drives deformation over time. Impacts near the line suggest a transitional regime in which both inputs contribute. The predominance of impacts above the brain's natural period suggests that rotational velocity plays a dominant role in brain deformation in this population. Holbourn's hypothesis, grounded in inertial loading experiments characteristic of indirect impacts, likely reflected longer-duration pulses, where the brain is more sensitive to rotational acceleration. This difference in loading conditions may account for the shift in sensitivity observed here.

### Linear acceleration is the most sensitive univariate determinant of concussion

Twelve kinematic and strain-based logistic regression models were developed to assess concussion classification performance and identify candidates for injury risk function development. Model deviance ( $G^2$ ), Bayesian Information Criterion, LASSO-penalized logistic regression, and dominance analysis were used to screen all candidate predictors. All models had significantly better fit than the null model, but the five models with the best fit were  $a + \omega$ ,  $a + \alpha$ ,  $a$ ,  $\alpha$ , and  $\omega$  based on the lowest deviance and Bayesian Information Criterion (Fig. 3a). Additionally,  $a$ ,  $\omega$ , and  $\alpha$  were consistently the most informative and best-fitting predictors across both LASSO and dominance analyses, based on having the largest  $R^2$  and general dominance scores, respectively (Extended Data Tables 8-9). Therefore,  $a + \omega$ ,  $a + \alpha$ ,  $a$ ,  $\alpha$ , and  $\omega$  were retained for formal statistical comparison as classifiers and for injury risk function development. This approach both preserved statistical power and enabled us to test our primary hypothesis that rotational acceleration is a more precise predictor of concussion than linear acceleration.

Model	Peak linear acceleration (a)	Peak rotational acceleration ( $\alpha$ )	Peak rotational velocity ( $\omega$ )	Peak linear acceleration + peak rotational velocity ( $a + \omega$ )	Peak linear acceleration + peak rotational acceleration ( $a + \alpha$ )
<b>AUPRC [95% CI]<sup>1</sup></b>	0.65 [0.27, 0.90]	0.36 [0.12, 0.67]	0.35 [0.07, 0.67]	0.64 [0.29, 0.90]	0.60 [0.24, 0.90]
<b>F1 [95% CI]<sup>1</sup></b>	0.50 [0.18, 0.80]	0.31 [0.13, 0.59]	0.30 [0.13, 0.57]	0.4 [0.22, 0.77]	0.55 [0.25, 0.8]
<b>Precision<sup>1</sup></b>	0.80	0.33	0.33	1.0	0.5
<b>Recall<sup>1</sup></b>	0.38	0.25	0.25	0.25	0.63
<b>Recall (Youth)<sup>2</sup></b>	0	0	0	0	0
<b>Decision Threshold<sup>1</sup></b>	0.2 (78.7 g)	0.1 (5874.2 rad/s <sup>2</sup> )	0.1 (29 rad/s)	0.3	0.1

1: Held-out set, 2: Youth set

**Table 1.** Performance metrics for logistic regression-based injury risk functions. The first test was conducted on the 20% held-out dataset, while recall (sensitivity) was calculated for the dataset containing 4 youth concussions.

Table 1 summarizes the classification performances on the youth and held-out test sets. No concussions were detected on the youth set. On the held-out set, **a** achieved the highest area under the precision–recall curve (AUPRC, 0.65) and F1 score (0.50). Among univariate models, **a** was followed by  $\alpha$  (AUPRC=0.36; F1=0.31) and  $\omega$  (AUPRC=0.35; F1=0.30). Differences between **a** and  $\alpha$  are significant (Figs. 3b-3c). Additionally, **a** +  $\alpha$  (AUPRC=0.60; F1=0.55) offered no detectable improvement over the use of **a** alone. Among bivariate models, **a** +  $\omega$  had the largest AUPRC (AUPRC = 0.64, F1 = 0.40), and significantly outperformed  $\alpha$  and  $\omega$  (Fig. 3b). It is important to note that the AUPRC of a random classifier, defined as the ratio of positive cases to total cases, is only 0.01, indicating that kinematic metrics alone still provide substantial discriminatory power. Dominance analysis and LASSO further confirmed **a** as the most informative predictor variable, with the highest general dominance score ( $R^2=0.108$ ) and LASSO coefficient ( $\beta=0.91$ ), followed by  $\omega$  ( $R^2 = 0.065$ ;  $\beta=0.842$ ) and  $\alpha$  ( $R^2 = 0.061$ ;  $\beta=0.380$ ).

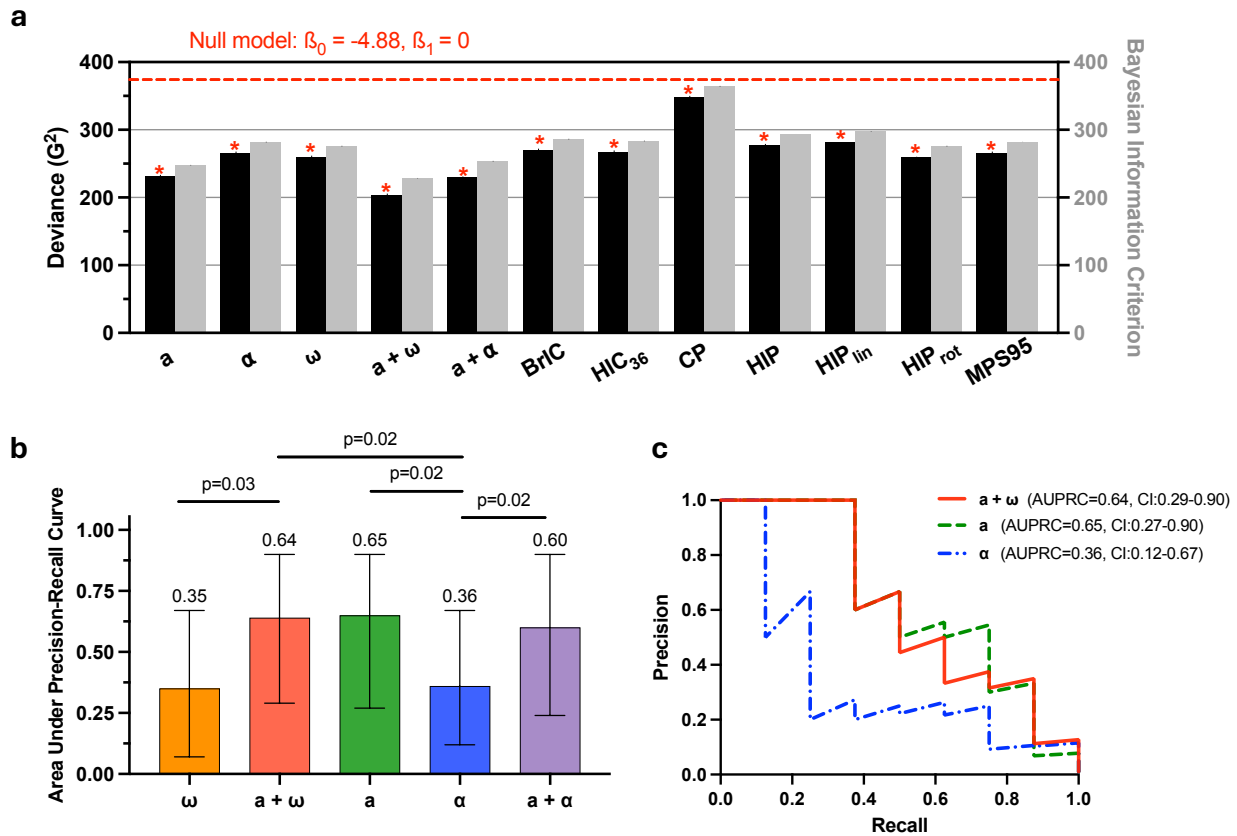


**Figure 3.** Comparison of model fit and performance for concussion classifiers. Model abbreviations are provided in Extended Data Table 4. **a**, In-sample goodness-of-fit for each model. A lower deviance ( $G^2$ ) indicates better fit relative to the null model, and all models provided significantly better fit compared to the null model (\*  $p < 0.005$ ). Bayesian Information Criterion assesses the tradeoff between model fit and complexity, with lower values indicating better performance while penalizing for model complexity. **b**, Area under the precision–recall curve for kinematic models, evaluated on the held-out test set. Black error bars represent 95% confidence intervals. **c**, Precision–recall curves for kinematic classifiers on the held-out test set.

Several additional metrics used in automotive and helmet safety assessments were evaluated, including MPS95, Brain Injury Criterion (BrIC),<sup>21</sup> Head Injury Criterion (HIC<sub>36</sub>),<sup>33</sup> Head Impact Power (HIP),<sup>34</sup> split into linear and rotational components, and Virginia Tech Combined Probability (CP)<sup>35</sup> (Extended Data Table 5). Although linear HIP outperformed rotational HIP based on AUPRC and F1, neither model achieved better fit than the five kinematic models described above. MPS95 and BrIC were among the lowest performers. As a result, these metrics were not used to construct injury risk functions or included in formal statistical comparisons.

### Linear acceleration shows a significant association with concussion risk

The five kinematic models identified by best fit were then used to develop injury risk functions. As described above, these included three univariate models ( $a$ ,  $\omega$ ,  $\alpha$ ) and two bivariate models ( $a + \alpha$  and  $a + \omega$ ). Model coefficients are provided in Extended Data Table 6, and the resulting risk functions are shown in Figure 4. The 50% injury risk thresholds were determined to be 99 g for  $a$ , 8,254 rad/s<sup>2</sup> for  $\alpha$  and 39 rad/s for  $\omega$  (Fig. 4a–4c).

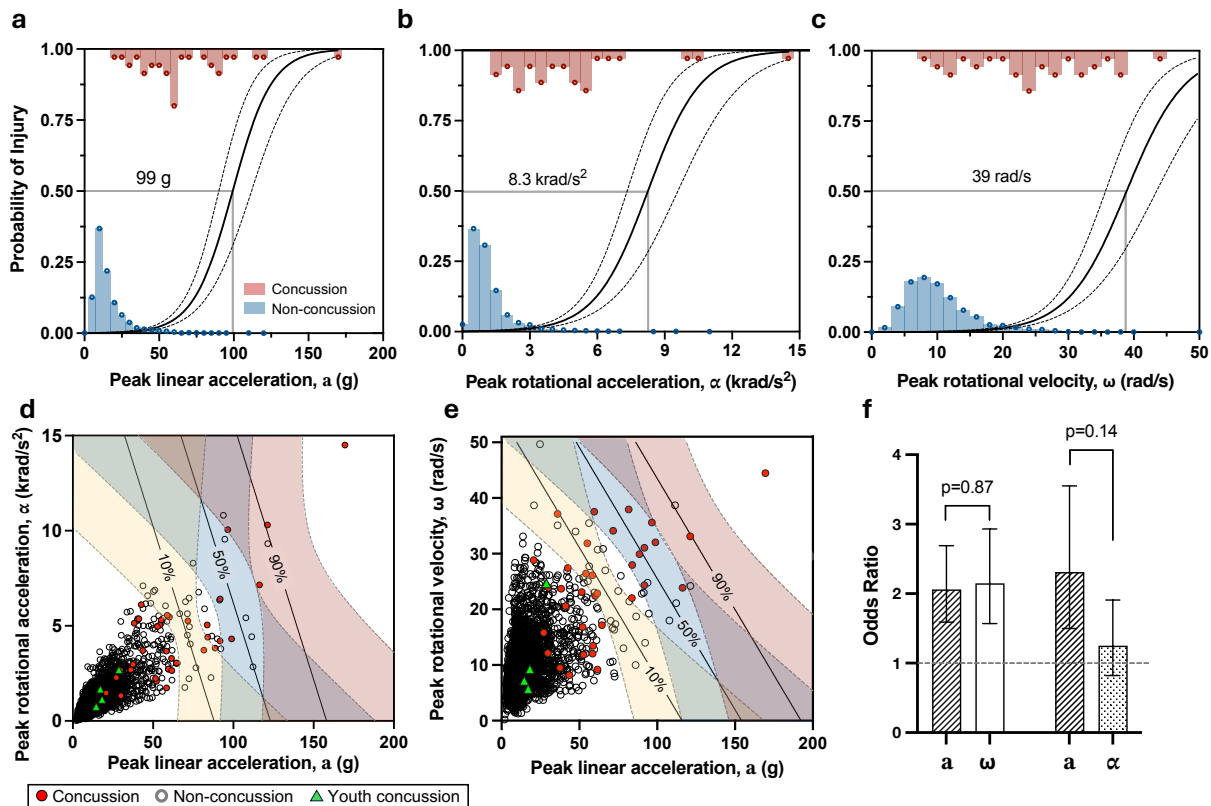


**Figure 4.** Injury risk functions developed on the 80% training data. Univariate logistic regression models based on **a**, peak linear acceleration, **b**, peak rotational acceleration, and **c**, peak rotational velocity. Solid black lines indicate the fitted logistic regression curves and dashed lines show the 95% confidence intervals. Injury risk functions for **d**,  $a + \alpha$  and **e**,  $a + \omega$ . The black contours and shaded regions indicate different risk levels and their 95% confidence intervals. Youth concussions are overlaid for comparison and did not contribute to the training data. **f**, Odds ratios plotted for each predictor in bivariate kinematic models. In the  $a + \alpha$  model, the confidence interval for  $\alpha$  crosses the reference line at  $y=1$ , indicating it is not a significant independent predictor of concussion.



Next, bivariate models allowed us to assess the relative importance of linear versus rotational terms. In the  $\alpha + \omega$  model, the 50% risk contour displayed a steep slope, suggesting greater sensitivity to  $\alpha$ . Consistent with this, odds ratios (OR) indicated  $\alpha$  was a significant independent predictor of concussion (OR = 2.3; 95% CI: 1.5-3.6), while  $\omega$  was not (OR = 1.3; 95% CI: 0.81-1.9), as its confidence interval included 1. The larger odds ratio for  $\alpha$  indicates it is a greater risk factor for concussion than  $\omega$ . However, the Wald test comparing the two ORs was not statistically significant (Fig. 4f). In the  $\alpha + \omega$  model, risk increased comparably with both predictors, as reflected by their similar odds ratios (OR $_{\alpha}$  = 2.1; OR $_{\omega}$  = 2.2) with no significant differences (Fig. 4f).

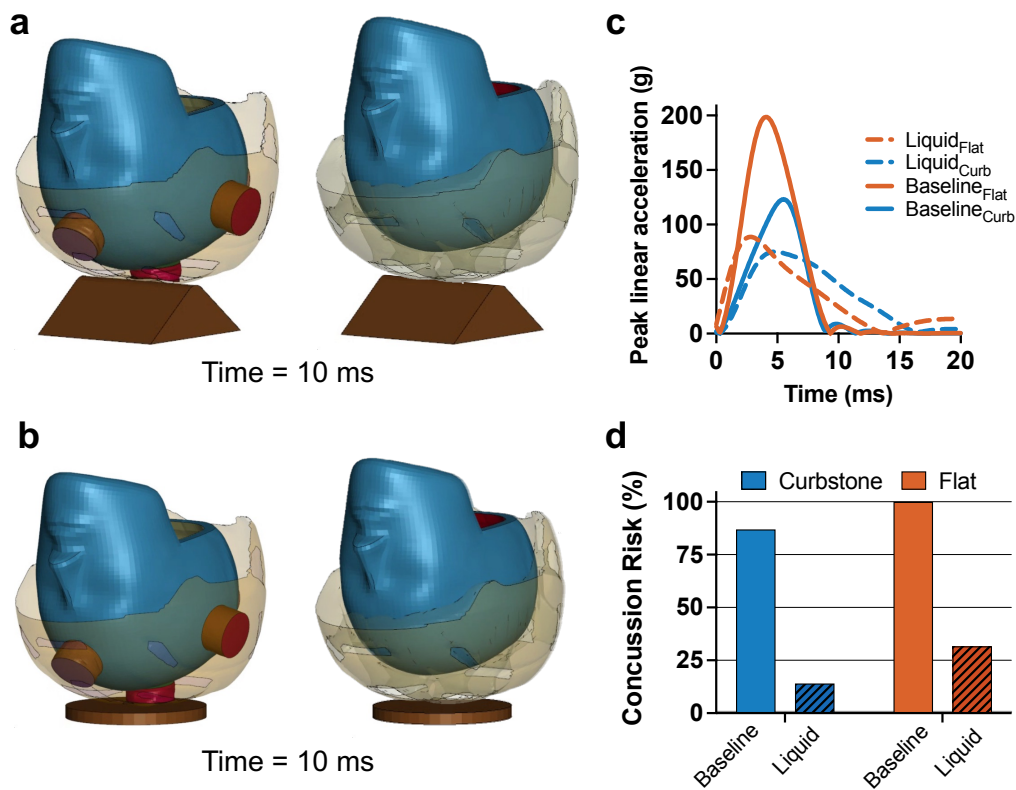


**Figure 5.** Comparison of liquid and baseline cycling helmets tested to the EN1078 certification standard. Impacts to the **a**, curbstone anvil and **b**, flat anvil at the top location of the liquid and baseline helmets at 10 ms, demonstrating differences in liner compression. The liquid shock absorbers undergo greater compression than the standard foam. Both helmets are fitted to a 50th percentile male Hybrid III headform. The red dashed line marks the apex of the head at t=1 ms. **c**, Peak linear acceleration traces for drop tests, filtered at 200 Hz. **d**, Injury risk derived from peak linear accelerations achieved in **c**.

### Liquid shock absorbers reduce concussion risk

We designed a finite element model of a cycling helmet with cylindrical liquid shock absorbers and evaluated its effectiveness in reducing linear acceleration concussion risk. A conventional cycling helmet with an expanded polystyrene liner served as the geometric basis and baseline helmet for comparison. During curbstone drop impacts

at 4.48 m/s (Fig. 5a), the liquid helmet reduced peak linear acceleration to 75 g, well below the EN1078 certification standard's pass/fail threshold of 250 g and our 50% risk threshold of 99 g, while the baseline helmet reached 125 g. In flat anvil impacts at 5.24 m/s (Fig. 5b), the liquid helmet achieved a peak linear acceleration of 88 g compared to 198 g for the baseline. Across impact conditions, this corresponded to a 73% and 68% reduction in predicted concussion risk relative to the baseline helmet. (Fig. 5d).

## Discussion

The rotational acceleration hypothesis for concussion has long guided brain injury prevention research, shaping safety standards and the development of protective equipment. Yet, this hypothesis has not been tested using direct measurements of rotational acceleration during concussion in humans due to limited data. We addressed this gap by collecting a dataset of directly measured rotational accelerations during human concussions using instrumented mouthguards across multiple sports and age groups. Surprisingly, we found linear acceleration to be a significantly more precise predictor of concussion than rotational acceleration. We developed a new injury risk function using peak linear acceleration and found that a standard cycling helmet is predicted to result in nearly 100% concussion risk under standard impact conditions. In comparison, our bio-inspired, liquid cycling helmet reduced linear accelerations and corresponding concussion risk by up to 73%. These findings suggest safety standards should incorporate linear acceleration set at lower thresholds to improve public safety.

We found peak linear acceleration to be a significantly more precise predictor of concussion than peak rotational acceleration. Peak linear acceleration ( $a$ ) was also the largest risk factor for concussion and the only significant contributor in the  $a + \alpha$  model (Fig. 4d). This was further supported by the dominance analysis and LASSO-penalized logistic regression where  $a$  contributed the most unique and stable predictive signal across both methods. A similar finding was observed in elite men's rugby union using iMGs, where peak linear acceleration was significantly associated with player removal for head injury assessment due to suspected concussion, while peak rotational acceleration was not.<sup>36</sup> However, the rugby study was limited by the use of receiver operating characteristic curves for evaluating predictive performance, which does not assess positive predictive value (i.e., precision). In datasets with a low concussion incidence such as the rugby study (58 removals, 5,400 non-removals), the area under the receiver operating characteristic curve is less informative because it gives equal weight to both classes and can be dominated by correct predictions of the much larger negative class. In contrast, we used precision–recall, which focuses on evaluating positive predictive value and sensitivity, and offers a more balanced evaluation of the classifier's performance on rare outcomes like concussion.

Likewise, a previous study using HITS football data reported better predictive performance for peak linear acceleration compared to peak rotational acceleration on a dataset of 244 concussions and 62,767 non-concussions.<sup>35</sup> However, to address underreporting, the concussion dataset in the HITS study included non-concussive impacts that were relabeled as concussions based on having large kinematic magnitudes. Additionally, there were no significant differences between peak linear acceleration and peak rotational acceleration in a separate test dataset on professional football impact reconstructions.<sup>35</sup> The HITS study similarly quantified predictive performance using receiver operating characteristic curves, which appear inflated by the correct classification of the majority class of non-concussions. These factors limit the ability of the HITS study to directly assess the predictive value of rotational acceleration for diagnosed concussions.

An intriguing outcome of the current study is that strain-based and composite injury metrics underperformed simple kinematic measures. We evaluated 95<sup>th</sup> percentile maximum principal strain (MPS95) and Brain Injury Criterion (BrIC) which are commonly used in research and regulatory settings. MPS95 is the target output of the Diffuse Axonal Multi-Axis General Evaluation (DAMAGE) model, a second-order system for estimating maximum brain strain used in the European New Car Assessment Program safety rating.<sup>37</sup> The National Football League also uses DAMAGE alongside the Head Injury Criterion (HIC<sub>36</sub>), which is based on linear acceleration, to calculate Helmet Performance Score for helmet safety rankings. Although the Helmet Performance Score has been shown to correlate with on-field concussion incidence, we found that MPS95 had low classification performance compared to kinematic metrics, including HIC<sub>36</sub> (Extended Data Table 5). Given that HIC<sub>36</sub> performed well and similarly to peak linear acceleration in our dataset, the observed correlation of Helmet Performance Score with concussion incidence may be driven by the linear acceleration component of HIC<sub>36</sub> rather than DAMAGE. Alternatively, the relatively low performance of MPS95 may reflect limitations in brain model fidelity, as strain-based bicycle helmet rankings have been shown to differ widely across models,<sup>38</sup> suggesting our findings may be model-dependent. Regional strain metrics have also been shown to improve classification,<sup>39</sup> though we only evaluated global MPS95 here. BrIC, a rotational velocity-based metric proposed by the National Highway Traffic Safety Association for automotive crash testing, has similarly informed helmet safety evaluations.<sup>40</sup> BrIC had the lowest predictive performance in our analysis (Extended Data Table 5). Prior work has shown that the critical rotational velocity thresholds used in BrIC can be exceeded during voluntary head motions without producing injurious brain strain.<sup>41</sup> This may have led to false positives during classification, which could explain BrIC's lower performance here.

The stronger predictive ability of linear acceleration is a surprising result that may stem from several factors. One possible explanation is that linear power was nearly eight times greater than rotational power across all impacts

(Fig. 1b, Extended Data Table 5), indicating that translational motion contributes more to the total mechanical energy transferred to the head. We also speculate one biomechanical mechanism by which linear acceleration could directly contribute to concussion: due to the slight density difference between the brain and cerebrospinal fluid (CSF), large linear acceleration of the skull may cause differential motion of the brain as it inertially lags behind. At lower linear accelerations, CSF may act as a shock absorber by resisting relative brain motion through its inertia. However, at higher accelerations, differential brain motion could compress the subarachnoid space and rapidly displace CSF through available outflow pathways such as the foramen magnum, thereby limiting its shock-absorbing capacity and potentially contributing to injury of surrounding structures. We speculate that this displacement might lead to injury due to direct contact between the brain and the inner skull at the coup site. Simultaneously, negative pressure at the contrecoup site could induce cavitation, a phenomenon in which vapor bubbles form and collapse within the CSF, blood, or parenchyma due to rapid pressure changes. Because pressure has shown to correlate strongly with linear acceleration,<sup>11</sup> this mechanism may be relevant in high-acceleration impacts. Cavitation is also a leading hypothesis for TBI from military blast exposure,<sup>42–44</sup> which could support linear acceleration as a unifying theory for blast-related brain injuries and concussion. However, this warrants future investigation as there is limited evidence supporting the occurrence of cavitation *in vivo* during concussion. Future studies should investigate brain displacement and pressure gradients during pure linear acceleration using fluid-structure interaction models,<sup>45,46</sup> as most models treat CSF as a solid and may not capture this behavior. Overall, while we do not dispute that rotational acceleration can cause of diffuse brain injury, our findings suggest that alternative or as-yet-unidentified mechanisms may warrant further investigation.

We derived a 50% concussion risk threshold of approximately 100 g (95% CI: 89g–110g) for peak linear acceleration (Fig. 4a). This threshold falls in between prior estimates based on on-field studies. Pellman et al. reported a lower 50% risk level of 85 g based on laboratory reconstructions of 31 impacts (25 concussions, 6 non-concussions) from the National Football League.<sup>47</sup> This could be attributed to the inflated concussion incidence which introduces selection bias, potentially overestimating the model's ability to distinguish between concussion and non-concussion cases and skewing the risk curve toward lower thresholds. The lower threshold may also reflect methodological limitations of laboratory reconstructions, such as idealized impact conditions and reliance on video resolution for kinematic accuracy. Similarly, McIntosh and colleagues reported a lower 50% risk threshold of 65 g in Australian football using computational multibody reconstructions of 40 impacts (27 concussions, 13 non-concussions),<sup>48</sup> where overrepresentation of concussive cases likely contributed to a risk function biased toward lower accelerations. By contrast, HITS data estimated 50% concussion risk at 192 g<sup>22</sup> which is much higher than

our observed threshold. This discrepancy may be due to noise introduced by relative motion between the helmet and skull, or the use of a higher filter cutoff frequency (1000 Hz), which could have preserved high-frequency signal or noise components.<sup>23</sup> Additionally, high acceleration false positive impacts due to lack of visual-verification in the non-concussive data could have been present, potentially causing the logistic regression model to learn a decision boundary skewed toward higher magnitudes and shifting the estimated 50% risk threshold upward.

Currently, no safety standard includes linear acceleration as a concussion metric. The Fédération Équestre Internationale (FEI) recently proposed a 150 g peak linear acceleration threshold for concussion,<sup>49</sup> yet our model indicates this corresponds to a >99% probability of injury. A threshold below 100 g, if using 200 Hz filtering, would better reflect observed injury risk. Our cycling helmet simulations demonstrate the practical value of such criteria. Under EN1078 certification conditions,<sup>50</sup> which permit peak linear acceleration values up to 250 g, the liquid helmet reduced concussion risk from 87% (95% CI: 69-95%) to 14% (95% CI: 10-22%) during curbstone impacts, and from 99% (95% CI: 98-100%) to 32% (95% CI: 20-45%) during impacts to a flat anvil (Fig. 5d). This improved performance is due in part to greater compression of the liquid shock absorbers, which enables more stroke to be utilized as the head decelerates. As the shock absorbers compress, fluid is forced through a fixed orifice, and pressure builds in proportion to the flow rate and orifice area (Eq. 8). This creates a regulated resistive force that remains steady throughout the stroke and reduces the sharp acceleration spike observed in the baseline helmet (Fig. 5c). The result is an extended impulse duration over which kinetic energy is dissipated, ultimately reducing concussion risk (Fig. 5d). The shock-absorbing effect of CSF may protect the brain in a similar manner though this warrants future investigation. CSF also may allow low-friction gliding between the brain and skull during head rotation. Reduction of friction on the head to minimize torque and rotation has been the primary goal of concussion prevention technologies that introduce slip liners into helmets.<sup>51</sup> Our results of linear acceleration as the most significant risk factor for concussion suggests that it may be even more important to minimize force than torque on the head. The current results overall suggest that linear impact mitigation technologies can meaningfully reduce concussion risk even within existing testing frameworks. Updating helmet standards to reflect concussion-relevant linear acceleration limits could therefore incentivize more effective protective equipment.

While our findings support incorporating peak linear acceleration thresholds into safety standards, rotational velocity-based metrics are often proposed as alternative or complementary measures. Although the  $\mathbf{a} + \boldsymbol{\omega}$  model achieved the highest AUPRC among bivariate models (Table 1), its implementation in helmet testing poses practical challenges. Induction of realistic peak rotational velocity requires oblique impacts, which are more complex and costly to execute than linear drop tests. Peak rotational velocity is also sensitive to the inclusion of the neck and

body,<sup>52</sup> and surface friction between the head and helmet. These variables are often excluded from standard helmet tests which typically involve isolated headforms. The absence of the full body may lead to underestimation of rotational velocity.<sup>52</sup> In contrast, automotive crash testing frequently employs full-body occupant models, making peak rotational velocity a better-suited metric in that context. However, the Hybrid III surrogate neck used in automotive tests was designed for frontal impacts, so the accuracy of rotational velocity during side or rear impacts remains uncertain. Future studies that perform helmet testing should consider full-body models to capture more complete rotational kinematics during helmet impacts.

To our knowledge, this is the first study to develop injury risk functions using concussion data that includes children and adult athletes of both sexes. While we did not conduct sex-specific analyses, this remains an important area for future research, particularly given existing evidence that females may be more susceptible to concussion than males.<sup>19</sup> Our dataset only included three female concussions from athletes in lacrosse, rugby, and women's artistic gymnastics. Additionally, youth concussions had much lower magnitudes compared to those from older athletes (Extended Data Table 2). The average peak linear acceleration was 16 g for youth and 68.3 g for non-youth concussions, while the average peak rotational acceleration was 1156 rad/s<sup>2</sup> for youth and 4919 rad/s<sup>2</sup> for the non-youth. During testing, the kinematic classifiers could not detect any youth concussions (Table 1), suggesting that much lower thresholds may be needed to accurately assess injury risk in youth athletes and develop effective helmets. Future work is needed to characterize kinematic and strain-based injury thresholds in youth populations using iMGs across a broad range of sports.

This study has several limitations that warrant consideration. First, while the liquid cycling helmet presented here reduced concussion risk by nearly half, physical prototypes and additional simulations for different impact locations on the helmet should be examined to fully evaluate performance. We also did not assess reductions in rotational velocity or rotational acceleration. Further, head impact data were collected using four different iMGs, each validated independently with device-specific filtering and cutoff frequencies. To ensure consistency across devices, kinematic traces were low-pass filtered at 200 Hz. This decision was guided by the fact that 47% of the dataset came from Prevent iMG data, which was only available with 200-Hz filtering. Additionally, different diagnostic criteria were used to include concussive impacts from multiple sources, which introduces variability (Extended Data Table 1). There is also a large difference, naturally, between the number of concussive versus non-concussive impacts in this study, which makes classification more challenging. Finally, the predictive accuracy of our thresholds and predicted reduction in concussion risk would need to be determined in a prospective study.

## Conclusion

This is the first study to use directly measured *in vivo* head kinematics from concussive impacts to show that linear acceleration is a more precise predictor of concussion than rotational acceleration. While rotational kinematics have guided concussion prediction due to the brain's susceptibility to shear forces, our findings suggest that linear motion plays a larger role in concussion biomechanics than previously recognized. Across a multi-center dataset of video-verified impacts collected from both male and female athletes, peak linear acceleration was the primary risk factor for concussion. We also found a 50% concussion risk threshold of approximately 100 g for peak linear acceleration, lower than any regulatory bodies have considered. Youth concussions occurred at much lower magnitudes and were not identified by kinematic classifiers, supporting the need for more research and lower, youth-specific thresholds. Finally, we showed that a bio-inspired, liquid-based cycling helmet can drastically reduce linear acceleration-associated concussion risk. Together, these findings support the incorporation and feasibility of linear acceleration thresholds below 100 g in concussion safety standards for non-youth populations.

## Methods

Mouthguard data was collated among cohorts from American football, Australian football, lacrosse, rugby union, artistic gymnastics, mixed martial arts, and ice hockey, where mouthguard sensors recorded linear and rotational head kinematics. Concussive impacts were identified based on diagnosis by trained personnel, athlete identification, or by visual signs of concussion confirmed by video reviewers. Video-verified impact kinematics were used to develop injury risk functions and estimate brain tissue-based criteria using finite element analysis. Injury prediction was investigated using univariate and bivariate logistic regression. Finally, a fluid-filled cycling helmet finite element model was developed and tested against our derived injury risk functions.

### Data description

A total of 3,805 non-concussive and 47 concussive impacts were compiled to construct the dataset for concussion risk modeling and classification (Extended Data Table 1). Concussions were either medically diagnosed or labeled based on visual signs of concussion observed during video review.<sup>53</sup> Kinematic data were collected with custom-fitted instrumented mouthguards, including the Prevent iMG,<sup>53</sup> the In-mouth ADXL/L3G4200D,<sup>54</sup> the Stanford MiG2.0,<sup>28</sup> the HITIQ Smart Mouthguard,<sup>26</sup> and the Wake Forest mouthpiece.<sup>55</sup> The dataset was sourced from youth ice hockey,<sup>56</sup> collegiate women's lacrosse, professional mixed martial arts,<sup>57</sup> women's advanced gymnastics,<sup>58</sup> amateur Australian football, and youth, high-school, and collegiate American football.<sup>53,59</sup> Among concussive impacts, 17 occurred in American football, 19 in Australian football, 5 in mixed martial arts, 3 in rugby union, 1 in gymnastics, 1 in ice hockey, and 1 in lacrosse. Three concussive impacts involved female athletes in lacrosse, rugby, and gymnastics. Youth was defined as below 14 years of age.

### Australian football, rugby union and lacrosse field data collection

Data collection methods for the published datasets included in our analysis are described in prior work (Extended Data Table 1), while collection methods for unpublished datasets are described here. The Australian football data builds on a 2022 two-team pilot study within the Victorian Amateur Football Association (VAFA) by Evans et al<sup>30</sup> and is primarily drawn from a broader VAFA cohort study investigating blood-based biomarkers of brain injury.<sup>60</sup> A subset of 11 men's teams (186 players) wore HITIQ iMGs over the 2022–2024 seasons to capture impacts exceeding an 8 g threshold. Video verification was conducted using the same procedures,<sup>30</sup> applied to all timestamped concussion cases and a subset of non-concussive impacts from selected matches, based on events passing HITIQ's filtering pipeline; data from verified cases were then reprocessed using a 200 Hz filter. Australian



football projects were approved by the Monash University Human Research Ethics Committee (Project IDs: 27684, 36297, 36556) and Deakin University (Project ID: 2022-337).

Additionally, as part of a larger ongoing study, the Prevent iMG was deployed to 21 collegiate rugby players (7 male, 14 female) on the Stanford rugby team to collect data for the complete 2022 season, while the Stanford MiG2.0 was deployed to 11 collegiate women's lacrosse players across 6 practices in the Spring 2018 season. All mouthguards were custom-fitted to the athlete's upper dentition and equipped with a triaxial accelerometer and triaxial gyroscope to record linear accelerations and rotational velocities during head impacts (Fig. 1a). Video footage was recorded at 4k resolution and 60 frames per second for all athlete-exposures using two camera angles to capture both halves of the field. A world clock was filmed at the start of the recording session to enable temporal synchronization between mouthguard-recorded events and session footage. All impacts exceeding a 10g trigger threshold were subject to visual verification, and only video-confirmed impacts were included in our analyses. Data collection was approved by the Stanford University Institutional Review Board (Protocol 45932).

### Kinematics processing

Kinematics for video-verified impacts measured with the Prevent, HITIQ, Stanford, and In-Mouth iMGs were first transformed to the SAE J211 coordinate system<sup>61</sup> (+X: forward, +Y, to the right, +Z downward). Linear acceleration and rotational velocity were then filtered using a fourth-order Butterworth low pass phaseless filter with a 200 Hz cutoff frequency. Rotational accelerations were next derived from rotational velocity measurements using a five-point stencil derivative and subsequently filtered at 200 Hz. Finally, linear accelerations were transformed to the head's center of gravity using the respective sensor locations for each mouthguard and Equation 1,

$$\mathbf{a}^{CG} = \mathbf{a}^{MG} + \alpha^{MG} \times \vec{r} + \omega^{MG} \times (\omega^{MG} \times \vec{r}) \quad (1)$$

where  $\mathbf{a}^{CG}$  is the linear acceleration (m/s<sup>2</sup>) at the head's center of gravity for a 50<sup>th</sup> percentile male,  $\mathbf{a}^{MG}$  is the linear acceleration of the mouthguard,  $\alpha$  is rotational acceleration (rad/s<sup>2</sup>),  $\omega$  is rotational velocity (rad/s), and  $\vec{r}$  is the constant distance vector from the accelerometer to the head's center of gravity. The 200 Hz frequency was chosen due to the unavailability of the raw kinematic data measured from the Prevent iMG in the American football dataset, which comprises 47% of our data. The sampling frequency of the iMGs used in this study are large enough such that a 200 Hz frequency cutoff avoids signal aliasing. Methods for evaluating measurement consistency across devices after 200 Hz filtering are provided in the Supplementary Information, and outcomes are shown in Extended Data Table 8 and Extended Data Figure 1. iMGs specifications are also provided in Extended Data Table 7.

Impacts that were measured by the Wake Forest mouthpiece followed a slightly different approach. First, data were filtered using a fourth-order Butterworth low pass phaseless filter with a 1,650 Hz cutoff frequency (CFC1000) for linear acceleration and a 250 Hz cutoff frequency for rotational velocity. The impact measured from the gymnastics participant was not initially filtered due to the lower 350 Hz sampling rate (Extended Data Table 7). The accelerometer baseline was zero-offset by subtracting the first data point from all subsequent samples. The gyroscope baseline was zero-offset by subtracting the fifth data point from all subsequent samples and setting the preceding 4 samples to zero. Data were then rotated to a conventional coordinate system (+X: forward, +Y, to the left, +Z upward). Rotational acceleration was derived from rotational velocity using the five-point stencil derivative method. Linear acceleration was then transformed to the head's center of gravity using Equation 1. For inclusion in this study, secondary filtering was applied with a 200 Hz cutoff frequency and data were re-rotated to follow the SAEJ211 coordinate system. For all iMGs, peak kinematic values were calculated from the resultant, or Euclidian norm, of the x, y and z directions.

Head impact power (HIP) is defined as the rate at which rotational and translational kinetic energy is transferred to the head, and was calculated using Equation 2,

$$HIP(t) = m \cdot a_x \int a_x dt + m \cdot a_y \int a_y dt + m \cdot a_z \int a_z dt + I_{xx} \cdot \alpha_x \cdot \omega_x + I_{yy} \cdot \alpha_y \cdot \omega_y + I_{zz} \cdot \alpha_z \cdot \omega_z \quad (2)$$

where m is head mass (kg),  $I_{xx}$ ,  $I_{yy}$ , and  $I_{zz}$  are the directional components of the head's moment of inertia ( $\text{kg} \cdot \text{cm}^2$ ), a is linear acceleration ( $\text{m/s}^2$ ),  $\alpha$  is rotational acceleration ( $\text{rad/s}^2$ ), and  $\omega$  is rotational velocity ( $\text{rad/s}$ ), further split into directional components. We used an average head mass of 4.1 kg and 3.2 kg for male and female athletes, respectively, based on cadaveric data.<sup>62,63</sup> The moments of inertia are described by equations 3-5.<sup>62,63</sup>

$$I_{xx}(\text{kg} \cdot \text{cm}^2) = 74.8m - 125.5 \quad (3)$$

$$I_{yy}(\text{kg} \cdot \text{cm}^2) = 72.4m - 90.2 \quad (4)$$

$$I_{zz}(\text{kg} \cdot \text{cm}^2) = 45.6m - 26.5 \quad (5)$$

## Data cleaning

All impacts included in this study underwent video verification to ensure impact timestamps aligned with visual events. For mixed martial arts, the concussive impact was defined as the impact with the highest

rotational acceleration recorded during the competitive event in which the concussion was diagnosed.<sup>57</sup> This method was used because head impacts occur frequently during competition, making it difficult to isolate a single concussive event when multiple potentially injurious impacts may occur in the same competitive bout. Additionally, one Australian football concussion was excluded since the infrared proximity sensor reading fell below the threshold used to classify true impacts and was therefore considered a false negative. Low proximity readings may reflect decoupling or recoupling between the mouthguard and upper dentition, which can produce noisy fluctuations or unusually low magnitudes relative to the observed head motion.<sup>15</sup> Therefore, this Australian football concussion was not included in the final dataset.

### **Finite element modeling of head impacts**

Maximum principal strains were computed using the Global Human Body Model Consortium 50<sup>th</sup> percentile male head and brain model (GHBMC M50-H v6.1). Brain tissue responses from the GHBMC model were previously validated with cadaveric data.<sup>64</sup> Mouthguard data were transformed to align with the SAEJ211 coordinate system of the GHBMC model. Linear accelerations were applied to the head's center of gravity and rotational velocities were applied globally. The 95<sup>th</sup> percentile maximum principal strains (MPS95) were extracted regionally and globally using a custom MATLAB script. Considered brain regions included the corpus callosum, brainstem, midbrain, basal ganglia, cerebral white matter, upper gray matter, lower gray matter, thalamus and cerebellum.

### **Statistical methods**

#### *Kinematics and strain comparisons*

All statistical analyses and model development were performed in RStudio (2024.09.0+375). Differences in peak kinematics and MPS95 between concussive and non-concussive impacts were tested using a Wilcoxon Rank Sum test with a Bonferroni correction ( $n=7$ ,  $p<0.007$ ). Additionally, to evaluate consistency across sensor measurements after filtering, empirical cumulative distribution functions of peak linear acceleration, peak rotational velocity, and their peak frequencies were compared between iMGs using a Kolmogorov-Smirnov test (Extended Data Figure 1 and Table 8). Further details on the statistical comparisons are described in the Supplementary Information.

#### *Logistic regression models*

We employed logistic regression models in order to 1) quantify how biomechanical metrics relevant to sports and automotive safety classify concussion and 2) derive injury risk functions. We first divided the full dataset into an 80% training set ( $n=3,078$ ) and 20% held-out test set ( $n=744$ ) with a fixed random seed and stratified sampling

to preserve concussion incidence. Additionally, youth concussions from the Wake Forest cohorts were withheld as a separate test set. All model threshold tuning described below were performed on the training set alone.

On the training set, rare-events logistic models were fit using ReLogit to address small-sample bias inherent in maximum likelihood estimation when the outcome of interest is rare.<sup>65</sup> Twelve candidate models were tested, including peak linear acceleration ( $a$ ), peak rotational acceleration ( $\alpha$ ), peak rotational velocity ( $\omega$ ),  $a + \alpha$ ,  $a + \omega$ , peak total head impact power (HIP),<sup>34</sup> peak rotational power (HIP<sub>rot</sub>), peak linear power (HIP<sub>lin</sub>), Head Injury Criterion (HIC<sub>36</sub>),<sup>33</sup> Brain Injury Criterion (BrIC),<sup>21</sup> Combined Probability (CP),<sup>35</sup> and 95<sup>th</sup> percentile maximum principal strain (MPS95). Further justification on the candidate models is described in the Supplementary Information. A prior correction of 5.5 concussions per 1,000 impacts was applied to the intercept term, which is the assumed concussion rate in collegiate American football.<sup>66</sup> This correction reduces bias in baseline probability estimates without affecting the slope coefficients. Models were implemented using the Zelig() function, with standard errors clustered by subject ID to account for within-player correlation. Predictors were standardized to have a mean of 0 and standard deviation of 1. Model fit was assessed by deviance ( $G^2$ ) and Bayesian Information Criterion.

Classification thresholds were optimized on the training set by sweeping from 0 to 1 in increments of 0.1 to maximize F1. Determined thresholds were then applied to the 20% held-out test set and performance metrics—including area under the precision–recall curve (AUPRC), F1, precision, and recall—were estimated with 95% confidence intervals using a stratified bootstrap approach over 1,000 iterations. The same thresholds were applied to the held-out youth concussions ( $n=4$ ) and recall (sensitivity) was calculated.

### *Injury Risk Functions*

To determine which logistic regression models to analyze as injury risk functions and subject to statistical comparison, we performed an initial screening using deviance ( $G^2$ ), Bayesian Information Criterion, LASSO-penalized logistic regression, and dominance analysis.  $G^2$  and Bayesian Information Criterion were used to assess model fit, while LASSO and dominance analysis evaluated relative predictor importance based on coefficient magnitude and variance explained, respectively. Predictors or models that ranked highly across these approaches were selected for injury risk modeling and statistical comparison. Full methodological details on the LASSO and dominance analyses are provided in the Supplementary Information.

The final subset of features selected for injury risk function development included  $a$ ,  $\omega$ ,  $\alpha$ , and  $\alpha$  based on consistently ranking as the top three predictors across both LASSO regression and dominance analysis. These three features also demonstrated the strongest model fit ( $G^2$  and BIC) relative to other predictor variables. Therefore,

univariate injury risk functions included  $\mathbf{a}$ ,  $\alpha$ , and  $\omega$ , while bivariate functions included linear combinations of  $\mathbf{a}$  and  $\omega$  (Eq. 6) and  $\mathbf{a}$  and  $\alpha$  (Eq. 7),

$$\left( \frac{P_{inj}}{1 - P_{inj}} \right) = \beta_0 + \beta_1 \mathbf{a} + \beta_2 \omega \quad (6)$$

$$\left( \frac{P_{inj}}{1 - P_{inj}} \right) = \beta_0 + \beta_1 \mathbf{a} + \beta_2 \alpha \quad (7)$$

where  $\mathbf{a}$ ,  $\alpha$ , and  $\omega$  represent peak linear acceleration, peak rotational acceleration, and peak rotational velocity, respectively. Bivariate models were also used to assess the relative contribution of linear and rotational information for injury risk prediction, allowing us to directly test our hypothesis that rotational acceleration is more predictive of concussion than linear acceleration. To do this, odds ratios and their 95% confidence intervals were compared between the linear and rotational term for each bivariate model. Predictor variables were standardized to have a mean of 0 and a standard deviation of 1, enabling comparisons on a common scale. Odds ratios were defined as the exponentiated logistic regression coefficients for a one-standard-deviation increase in each predictor. The Wald Test was used to assess significant differences between odds ratios for bivariate models including a linear and rotational term, with a Bonferroni-adjusted significance level of  $p < 0.017$ . This approach allowed us to determine whether linear or rotational kinematics were more strongly associated with concussion outcome.

Additionally, we tested our hypothesis by comparing AUPRC values on the 20% held-out test set across the five kinematic models:  $\mathbf{a}$ ,  $\alpha$ ,  $\omega$ ,  $\mathbf{a} + \alpha$  (Eq. 6), and  $\mathbf{a} + \omega$  (Eq. 7). AUPRC differences between models were tested using the `pr.test` function in the `usefun` R package, which performs a stratified bootstrap comparison of precision-recall curves based on the Davis and Goadrich formulation.<sup>67</sup> A significance level of  $p < 0.05$  (two-tailed) was used. AUPRC was chosen due to the highly imbalanced nature of the dataset, as precision-recall more accurately reflects the model's capability to classify the minority class. Finally, sensitivity was assessed on a second held-out test set of four youth concussions to assess whether decision thresholds derived on adult and young adult data can detect youth injuries.

### Helmet modeling and impact simulations

We developed a finite element cycling helmet model incorporating liquid shock absorbers to evaluate their effectiveness in mitigating translational brain loading during head impacts. We have recently shown that liquid shock absorbers are a promising energy dissipation mechanism in American football helmets,<sup>68–70</sup> reducing head acceleration response metric (HARM) by 32% compared to conventional padding across standardized impact conditions. During impact, the absorber compresses axially and forces fluid through a narrow internal orifice,

generating resistance that slows the impacting mass at an approximately constant force. This behavior produces a velocity-dependent pressure drop across the orifice, described by Equation 8,

$$\Delta P = \frac{\rho Q^2}{2C_d^2 A_o^2} \quad (8)$$

where  $\rho$  is the fluid density (kg/m<sup>3</sup>),  $Q$  is the volumetric flow rate (m<sup>3</sup>/s),  $C_d$  is the discharge coefficient, and  $A_o$  is the orifice cross-sectional area (m<sup>2</sup>). For this study, the orifice area was set to 165 mm<sup>2</sup>.

All pre- and post-processing were performed in LS-PrePost 4.9, and simulations were conducted using a LS-DYNA double-precision solver (ls-dyna\_smp\_d\_R13\_1\_0\_x64\_centos79\_ifort190). A medium-sized Giro Caden cycling helmet served as the geometric and structural basis, and baseline helmet for comparison. Methods for 3D scanning and mesh generation to convert the physical helmet into a high-fidelity FE model are previously described by Abayazid et al.<sup>71</sup> The original expanded polystyrene liner (mass = 214.7 g) was removed and replaced with five cylindrical liquid shock absorbers positioned at the top, front, back, and lateral regions. The absorber walls were modeled as \*MAT\_FABRIC for the plain-weave high-strength fabric material ( $E = 76$  GPa,  $\rho = 777$  kg/m<sup>3</sup>) with carbon fiber endcaps and an internal water chamber, as described by Cecchi et al.<sup>68</sup> Absorber heights ranged from 30–35 mm, with individual masses between 37–43 g, totaling 195.9 g for all five absorbers.

The outer helmet shell was modified from a 3 mm polycarbonate material to a 0.5 mm carbon fiber composite (CF T700/2510)<sup>72</sup> for both the baseline and liquid helmet. Material properties were assigned using the \*MAT\_ELASTIC card, with Young's modulus set to 55 GPa and a density to 1500 kg/m<sup>3</sup>, compared to 2.5 GPa and 1200 kg/m<sup>3</sup> for polycarbonate. Nodal constraints were applied to tie the top surface of each absorber to the inner surface of the shell. The stiffer carbon fiber shell was necessary to engage the liquid shock absorbers upon impact, while the baseline helmet shell was modified to carbon fiber so that the shock absorbing liner material (liquid versus foam) was the only independent variable being tested.

The baseline and liquid helmet models were each fit to a 50th percentile Hybrid III male headform and subjected to drop impact simulations based on EN1078 certification standards.<sup>50</sup> Impacts were performed at the top location of the helmet, with initial velocities of 5.24 m/s and 4.48 m/s for flat and curbstone anvils, respectively. Peak linear acceleration was extracted from the head's center of gravity, then was subjected to the same filtering methods as described for the iMG data (see *Kinematics Processing section*) and used to compute injury risk.

## **Acknowledgements**

This work was supported by the Taube Stanford Children's Concussion Initiative, Pac-12 Conference's Student-Athlete Health and Well-Being Initiative, the National Institutes of Health (R24NS098518 and K25HD101686), the Stanford Maternal and Child Health Research Institute, the Office of Naval Research, and the National Science Foundation Graduate Research Fellowship Program. The authors want to thank Drs. Vahidullah Tac, Nicholas Cecchi, and Xianghao Zhan for providing help with the methodological approach. We also thank Drs. Lyndia Wu, Fidel Hernandez, Kaveh Laksari, Michael Fanton, Abigail Swenson, Ty Holcomb, and Madison Marks for data collection efforts. The authors thank Lauren Evans, Joel Ernest, William Zhou, Che Bonini, Mary-Anne Camenzuli, Luke Boykett, Jason Turner, Av Kumar, and Paul Kennedy for their Australian football data collection efforts. We thank Tie Liang for help with the statistical approach. We thank Praveen Sundar, Angel Gunaman, and Abigail Huddleston for assisting with video review. J.A.T. acknowledges the Stanford Graduate Fellowship and support from Stanford's Department of Bioengineering.

## **Author Contributions**

D.B.C. contributed to the conceptualization and initiation of the study. D.B.C., M.M.Z., S.J.M, and J.A.T. contributed to the methodological approach. M.M.Z and D.B.C initiated field data collection at Stanford. J.A.T. led the study design and performed all data analyses. F.F.A. created the finite element helmet model and performed the initial simulations. S.J.M oversaw the collection of Australian football data. J.W.H., W.T.O., and S.S.H.R. collected and processed the Australian football data. J.E.U., J.D.S., and N.S.P. contributed Wake Forest concussion data. N.S.P processed Wake Forest concussion kinematic data. J.A.T. wrote the manuscript. D.B.C. supervised the analysis and manuscript writing. All authors provided comments on the manuscript.

## **Competing Interests**

D.B. Camarillo is an inventor of the liquid shock absorbing technology which is owned by Stanford University and *SoftShox*. He is a founder of *SoftShox*, who is currently pursuing a license for this technology from Stanford. All other authors declare no competing interests.

## **Material and Correspondence**

Correspondence and requests for materials should be addressed to Jessica A. Towns (jtowns03@stanford.edu).

## **Data Availability**

The datasets analyzed during the current study are available from the corresponding author on reasonable request.

## References

1. Hodgson, V. R. & Thomas, L. M. Acceleration Induced Shear Strains in a Monkey Brain Hemisection. in 791023 (1979). doi:10.4271/791023.
2. Peerless, S. J. & Rewcastle, N. B. Shear injuries of the brain. *Can Med Assoc J* **96**, 577–582 (1967).
3. Zhao, W. & Ji, S. Real-time, whole-brain, temporally resolved pressure responses in translational head impact. *Interface Focus*. **6**, 20150091 (2016).
4. Kleiven, S. Why Most Traumatic Brain Injuries are Not Caused by Linear Acceleration but Skull Fractures are. *Front. Bioeng. Biotechnol.* **1**, (2013).
5. Dewan, M. C. *et al.* Estimating the global incidence of traumatic brain injury. *Journal of Neurosurgery* **130**, 1080–1097 (2019).
6. Blennow, K. *et al.* Traumatic brain injuries. *Nat Rev Dis Primers* **2**, 16084 (2016).
7. Tagge, C. A. *et al.* Concussion, microvascular injury, and early tauopathy in young athletes after impact head injury and an impact concussion mouse model. *Brain* **141**, 422–458 (2018).
8. Daneshvar, D. H. *et al.* Leveraging football accelerometer data to quantify associations between repetitive head impacts and chronic traumatic encephalopathy in males. *Nat Commun* **14**, 3470 (2023).
9. Hoge, C. W. *et al.* Mild Traumatic Brain Injury in U.S. Soldiers Returning from Iraq. *N Engl J Med* **358**, 453–463 (2008).
10. Holbourn, A. H. S. MECHANICS OF HEAD INJURIES. *The Lancet* **242**, 438–441 (1943).
11. Hardy, W. N. *et al.* A Study of the Response of the Human Cadaver Head to Impact. in 2007-22–0002 (2007). doi:10.4271/2007-22-0002.
12. Magdesian, M. H. *et al.* Atomic Force Microscopy Reveals Important Differences in Axonal Resistance to Injury. *Biophysical Journal* **103**, 405–414 (2012).
13. Ommaya, A. K., Hirsch, A. E., Flamm, E. S. & Mahone, R. H. Cerebral Concussion in the Monkey: An Experimental Model. *Science* **153**, 211–212 (1966).
14. Yarnell, P. & Ommaya, A. K. Experimental cerebral concussion in the rhesus monkey. *Bull N Y Acad Med* **45**, 39–45 (1969).
15. Gennarelli, T. A., Thibault, L. E. & Ommaya, A. K. Pathophysiologic Responses to Rotational and Translational Accelerations of the Head. in 720970 (1972). doi:10.4271/720970.



16. Cullen, D. K. *et al.* A Porcine Model of Traumatic Brain Injury via Head Rotational Acceleration. in *Injury Models of the Central Nervous System* (eds. Kobeissy, F. H., Dixon, C. E., Hayes, R. L. & Mondello, S.) vol. 1462 289–324 (Springer New York, New York, NY, 2016).
17. Hajiaghamemar, M. & Margulies, S. S. Multi-Scale White Matter Tract Embedded Brain Finite Element Model Predicts the Location of Traumatic Diffuse Axonal Injury. *J Neurotrauma* **38**, 144–157 (2021).
18. Smith, D. H. & Meaney, D. F. Axonal Damage in Traumatic Brain Injury. *Neuroscientist* **6**, 483–495 (2000).
19. Song, H. *et al.* Sex differences in the extent of acute axonal pathologies after experimental concussion. *Acta Neuropathol* **147**, 79 (2024).
20. Rowson, S. *et al.* A Six Degree of Freedom Head Acceleration Measurement Device for Use in Football. *Journal of Applied Biomechanics* **27**, 8–14 (2011).
21. Takhounts, E. G., Craig, M. J., Moorhouse, K., McFadden, J. & Hasija, V. Development of Brain Injury Criteria (BrIC). in 2013-22–0010 (2013). doi:10.4271/2013-22-0010.
22. Rowson, S. & Duma, S. M. Development of the STAR Evaluation System for Football Helmets: Integrating Player Head Impact Exposure and Risk of Concussion. *Ann Biomed Eng* **39**, 2130–2140 (2011).
23. Beckwith, J. G., Greenwald, R. M. & Chu, J. J. Measuring Head Kinematics in Football: Correlation Between the Head Impact Telemetry System and Hybrid III Headform. *Ann Biomed Eng* **40**, 237–248 (2012).
24. O'Connor, K. L., Rowson, S., Duma, S. M. & Broglio, S. P. Head-Impact–Measurement Devices: A Systematic Review. *Journal of Athletic Training* **52**, 206–227 (2017).
25. Rowson, B., Tyson, A., Rowson, S. & Duma, S. Measuring head impacts: accelerometers and other sensors. in *Handbook of Clinical Neurology* vol. 158 235–243 (Elsevier, 2018).
26. Stitt, D., Draper, N., Alexander, K. & Kabaliuk, N. Laboratory Validation of Instrumented Mouthguard for Use in Sport. *Sensors (Basel)* **21**, 6028 (2021).
27. Bartsch, A. J. *et al.* Laboratory and On-field Data Collected by a Head Impact Monitoring Mouthguard. in *2019 41st Annual International Conference of the IEEE Engineering in Medicine and Biology Society (EMBC)* 2068–2072 (IEEE, Berlin, Germany, 2019). doi:10.1109/EMBC.2019.8856907.
28. Liu, Y. *et al.* Validation and Comparison of Instrumented Mouthguards for Measuring Head Kinematics and Assessing Brain Deformation in Football Impacts. *Ann Biomed Eng* **48**, 2580–2598 (2020).
29. Cecchi, N. J. *et al.* Identifying Factors Associated with Head Impact Kinematics and Brain Strain in High School American Football via Instrumented Mouthguards. *Ann Biomed Eng* **49**, 2814–2826 (2021).

30. Evans, L. J. *et al.* Associations Between Instrumented Mouthguard-Measured Head Acceleration Events and Post-Match Biomarkers of Astroglial and Axonal Injury in Male Amateur Australian Football Players. *Sports Med* (2024) doi:10.1007/s40279-024-02138-6.
31. Krieger, L. Concussions: Stanford researchers use high-tech mouth guards to study head trauma in young athletes. *The Mercury News* (2018).
32. Gabler, L. F., Joodaki, H., Crandall, J. R. & Panzer, M. B. Development of a Single-Degree-of-Freedom Mechanical Model for Predicting Strain-Based Brain Injury Responses. *Journal of Biomechanical Engineering* **140**, 031002 (2018).
33. Newman, J. A. Head Injury Criteria in Automotive Crash Testing. in 801317 (1980). doi:10.4271/801317.
34. Newman, J. A. & Shewchenko, N. A Proposed New Biomechanical Head Injury Assessment Function - the Maximum Power Index. in 2000-01-SC16 (2000). doi:10.4271/2000-01-SC16.
35. Rowson, S. & Duma, S. M. Brain Injury Prediction: Assessing the Combined Probability of Concussion Using Linear and Rotational Head Acceleration. *Ann Biomed Eng* **41**, 873–882 (2013).
36. Allan, D. *et al.* Head Kinematics Associated with Off-Field Head Injury Assessment (HIA1) Events in a Season of English Elite-Level Club Men's and Women's Rugby Union Matches. *Sports Med* (2024) doi:10.1007/s40279-024-02146-6.
37. Brain injury calculation. (2022).
38. Fahlstedt, M. *et al.* Ranking and Rating Bicycle Helmet Safety Performance in Oblique Impacts Using Eight Different Brain Injury Models. *Ann Biomed Eng* **49**, 1097–1109 (2021).
39. Wu, S., Zhao, W., Rowson, B., Rowson, S. & Ji, S. A network-based response feature matrix as a brain injury metric. *Biomech Model Mechanobiol* **19**, 927–942 (2020).
40. Baker, C. E. *et al.* How Well Do Popular Bicycle Helmets Protect from Different Types of Head Injury? *Ann Biomed Eng* **52**, 3326–3364 (2024).
41. Hernandez, F. & Camarillo, D. B. Voluntary Head Rotational Velocity and Implications for Brain Injury Risk Metrics. *Journal of Neurotrauma* **36**, 1125–1135 (2019).
42. Moore, D. F. *et al.* Blast Physics and Central Nervous System Injury. *Future Neurol.* **3**, 243–250 (2008).
43. Franck, C. Microcavitation: the key to modeling blast traumatic brain injury? *Concussion* **2**, CNC47 (2017).
44. Panzer, M. B., Myers, B. S., Capehart, B. P. & Bass, C. R. Development of a Finite Element Model for Blast Brain Injury and the Effects of CSF Cavitation. *Ann Biomed Eng* **40**, 1530–1544 (2012).

45. Willinger, R. & Baumgartner, D. Human head tolerance limits to specific injury mechanisms. *International Journal of Crashworthiness* **8**, 605–617 (2003).
46. Zhou, Z., Li, X. & Kleiven, S. Fluid–structure interaction simulation of the brain–skull interface for acute subdural haematoma prediction. *Biomech Model Mechanobiol* **18**, 155–173 (2019).
47. Pellman, E. J., Viano, D. C., Tucker, A. M. & Casson, I. R. Concussion in Professional Football: Location and Direction of Helmet Impacts—Part 2. *Neurosurgery* **53**, 1328–1341 (2003).
48. McIntosh, A. S. *et al.* The biomechanics of concussion in unhelmeted football players in Australia: a case–control study. *BMJ Open* **4**, e005078 (2014).
49. *FEI HELMET WORKING GROUP TECHNICAL REPORT - NEW TESTING PROTOCOL*. (2023).
50. EN B. 1078. Helmets for pedal cyclists and for users of skateboards and roller skates.
51. Bottlang, M., Rouhier, A., Tsai, S., Gregoire, J. & Madey, S. M. Impact Performance Comparison of Advanced Bicycle Helmets with Dedicated Rotation-Damping Systems. *Ann Biomed Eng* **48**, 68–78 (2020).
52. Fahlstedt, M., Kleiven, S. & Li, X. Current playground surface test standards underestimate brain injury risk for children. *Journal of Biomechanics* **89**, 1–10 (2019).
53. Bartsch, A. J. *et al.* High Energy Side and Rear American Football Head Impacts Cause Obvious Performance Decrement on Video. *Ann Biomed Eng* **48**, 2667–2677 (2020).
54. Camarillo, D. B., Shull, P. B., Mattson, J., Shultz, R. & Garza, D. An Instrumented Mouthguard for Measuring Linear and Angular Head Impact Kinematics in American Football. *Ann Biomed Eng* **41**, 1939–1949 (2013).
55. Rich, A. M. *et al.* Development, Validation and Pilot Field Deployment of a Custom Mouthpiece for Head Impact Measurement. *Ann Biomed Eng* **47**, 2109–2121 (2019).
56. Swenson, A., Miller, L., Urban, J. & Stitzel, J. Head Kinematics by Contact Scenarios in Youth Ice Hockey. *Neurology* **95**, (2020).
57. Tiernan, S. *et al.* Concussion and the severity of head impacts in mixed martial arts. *Proc Inst Mech Eng H* **234**, 1472–1483 (2020).
58. Pritchard, N. S., E. Urban, J., Miller, L. E., Lintner, L. & Stitzel, J. D. AN ANALYSIS OF HEAD KINEMATICS IN WOMEN'S ARTISTIC GYMNASTICS. *SGJ* **12**, 229–242 (2020).
59. Hernandez, F. *et al.* Six Degree-of-Freedom Measurements of Human Mild Traumatic Brain Injury. *Ann Biomed Eng* **43**, 1918–1934 (2015).
60. O'Brien, W. T. *et al.* Next-Day Serum Glial Fibrillary Acidic Protein Levels to Aid Diagnosis of Sport-Related Concussion. *Neurology* **104**, (2025).

61. Safety Test Instrumentation Stds Comm. Sign Convention for Vehicle Crash Testing. doi:10.4271/J1733\_201811.
62. Connor, T. A., Stewart, M., Burek, R. & Gilchrist, M. D. Influence of headform mass and inertia on the response to oblique impacts. *International Journal of Crashworthiness* **24**, 677–698 (2019).
63. Tierney, G. *et al.* Identifying a severity measure for head acceleration events associated with suspected concussions. Preprint at <https://doi.org/10.48550/ARXIV.2410.01343> (2024).
64. Lyu, D., Zhou, R., Lin, C., Prasad, P. & Zhang, L. Development and Validation of a New Anisotropic Visco-Hyperelastic Human Head Finite Element Model Capable of Predicting Multiple Brain Injuries. *Front. Bioeng. Biotechnol.* **10**, 831595 (2022).
65. King, G. & Zeng, L. Logistic Regression in Rare Events Data. *Polit. anal.* **9**, 137–163 (2001).
66. Rowson, S., Brolinson, G., Goforth, M., Dietter, D. & Duma, S. Linear and Angular Head Acceleration Measurements in Collegiate Football. *Journal of Biomechanical Engineering* **131**, 061016 (2009).
67. Davis, J. & Goadrich, M. The relationship between Precision-Recall and ROC curves. in *Proceedings of the 23rd international conference on Machine learning - ICML '06* 233–240 (ACM Press, Pittsburgh, Pennsylvania, 2006). doi:10.1145/1143844.1143874.
68. Cecchi, N. J., Vahid Alizadeh, H., Liu, Y. & Camarillo, D. B. Finite element evaluation of an American football helmet featuring liquid shock absorbers for protecting against concussive and subconcussive head impacts. *Front. Bioeng. Biotechnol.* **11**, 1160387 (2023).
69. Vahid Alizadeh, H., Fanton, M. G., Domel, A. G., Grant, G. & Camarillo, D. B. A Computational Study of Liquid Shock Absorption for Prevention of Traumatic Brain Injury. *Journal of Biomechanical Engineering* **143**, 041008 (2021).
70. Cecchi, N. J. *et al.* A wearable hydraulic shock absorber with efficient energy dissipation. *International Journal of Mechanical Sciences* **270**, 109097 (2024).
71. Abayazid, F. F. & Ghajari, M. Viscoelastic circular cell honeycomb helmet liners for reducing head rotation and brain strain in oblique impacts. *Materials & Design* **239**, 112748 (2024).
72. Liu, Z., Zou, K. & Zhang, Z. Energy Absorption Behavior of Carbon-Fiber-Reinforced Plastic Honeycombs under Low-Velocity Impact Considering Their Ply Characteristics. *Materials* **17**, 4257 (2024).

## Extended Data

**Extended Data Table 1.** Head impact datasets used in this study.

Authors	Sport	Level(s)	Gender(s)	Measurement Device	No. Concussions	No. Non-concussions	Diagnostic criteria
Current study	Lacrosse	Collegiate	Female	Stanford MiG2.0	1	102	Immediate diagnosis
Current study	Rugby	Collegiate	Female/ Male	Prevent iMG	3	469	Immediate diagnosis/ player identification of impact
Domel et al. <sup>1</sup>	American football	Collegiate	Male	Stanford MiG2.0	0	359	
Hernandez et al. <sup>2</sup>	American football	Collegiate	Male	In-Mouth (ADXL377/L3G4200D)	1	0	Immediate diagnosis
Bartsch et al. <sup>3</sup>	American football	High-school, collegiate	Male	Prevent iMG	13	1782	Visual signs of concussion
Tiernan et al. <sup>4</sup>	Mixed martial arts	Professional, semi-professional, amateur	Male	Stanford MiG 2.0	5	304	Largest $\alpha$ impact immediately prior to diagnosis
Evans et al. <sup>5</sup> and ongoing study	Australian football	Amateur	Male	HITIQ	19	776	Immediate diagnosis
NIH Grant K25HD101686	American football	Youth	Male	WF	3	0	Immediate diagnosis
Pritchard et al. <sup>6</sup>	Gymnastics	Advanced	Female	WF	1	0	Immediate diagnosis
Swenson et al. <sup>7</sup>	Ice hockey	Youth	Male	WF	1	0	Immediate diagnosis

**Extended Data Table 2.** Kinematics summary statistics for concussive and non-concussive impacts.

	Concussion								Non-concussion			
	Mean		Median		95th%		SD		Mean	Median	95th%	SD
	Non-Youth	Youth	Non-Youth	Youth	Non-Youth	Youth	Non-Youth	Youth	Non-Youth	Non-Youth	Non-Youth	Non-Youth
<b>a (g)</b>	68.3	19.7	60.2	17.6	120.7	27.2	32.2	6.2	16.0	12.6	39.0	11.7
<b><math>\alpha</math> (rad/s<sup>2</sup>)</b>	4919	1560	4315	1399	10281	2536	3402	841	1156	899	2941	956
<b><math>\omega</math> (rad/s)</b>	24.6	11.7	23.9	8.2	43.1	22.4	9.8	8.8	10.2	9.2	20.3	5.1
<b>HIP<sub>total</sub> (kW)</b>	10	0.78	8.4	0.79	31.7	1.1	8.9	0.33	1.0	0.6	3.7	1.7
<b>HIP<sub>lin</sub> (kW)</b>	9.5	0.67	8.1	0.76	27.5	0.82	8.6	0.22	1.0	0.5	3.5	1.6
<b>HIP<sub>rot</sub> (kW)</b>	1.5	0.26	1.1	0.09	4.7	0.7	1.8	0.37	0.1	0.1	0.4	0.2

**Extended Data Table 3.** Regional strain summary statistics for concussive and non-concussive impacts.

	Concussion				Non-concussion			
	Mean	Median	95th%	SD	Mean	Median	95th%	SD
<b>Global</b>	0.32	0.32	0.70	0.18	0.12	0.11	0.26	0.07
<b>White matter</b>	0.30	0.30	0.65	0.17	0.12	0.10	0.26	0.07
<b>Upper gray matter</b>	0.36	0.35	0.80	0.21	0.14	0.12	0.29	0.08
<b>Lower gray matter</b>	0.20	0.20	0.39	0.11	0.08	0.07	0.16	0.04
<b>Thalamus</b>	0.27	0.24	0.56	0.20	0.08	0.07	0.18	0.06
<b>Brainstem</b>	0.23	0.21	0.44	0.16	0.06	0.15	0.04	0.08
<b>Corpus callosum</b>	0.48	0.36	1.28	0.41	0.11	0.08	0.27	0.10
<b>Basal ganglia</b>	0.28	0.26	0.54	0.16	0.10	0.09	0.22	0.06
<b>Cerebellum</b>	0.13	0.13	0.21	0.07	0.04	0.04	0.09	0.02

**Extended Data Table 4.** Kinematic and strain-based model abbreviations referenced in this study.

<b>Metric</b>	<b>Abbreviation</b>
Peak linear acceleration	<b>a</b>
Peak rotational velocity	<b><math>\omega</math></b>
Peak rotational acceleration	<b><math>\alpha</math></b>
95th percentile maximum principal strain	MPS95 (%)
Head injury criterion <sup>8</sup>	HIC <sub>36</sub>
Brain injury criterion <sup>9</sup>	BrIC
Combined probability <sup>10</sup>	CP
Head impact power <sup>11</sup>	HIP (kW)
Linear head impact power	HIP <sub>lin</sub> (kW)
Rotational head impact power	HIP <sub>rot</sub> (kW)

**Extended Data Table 5.** Performance metrics for additional kinematic- and strain-based classifiers.

Metric	AUPRC	F1	Precision	Recall
MPS95	0.28	0.29	0.33	0.25
HIP	0.51	0.50	0.75	0.38
HIP <sub>lin</sub>	0.51	0.50	0.75	0.38
HIP <sub>rot</sub>	0.39	0.35	0.50	0.25
HIC <sub>36</sub>	0.60	0.36	0.66	0.25
BrlC	0.18	0.25	0.22	0.25
CP	0.45	0.36	0.67	0.25

**Extended Data Table 6.** Coefficients for injury risk functions.

Model	Intercept	B1	B2
Peak linear acceleration	-8.363	0.0904	-
Peak rotational acceleration	-6.966	0.00084	-
Peak rotational velocity	-8.785	0.2353	-
Peak linear acceleration + peak rotational velocity	-9.946	0.0741	$1.38 \times 10^{-1}$
Peak linear acceleration + peak rotational acceleration	-8.327	0.0949	$-7.89 \times 10^{-5}$

**Extended Data Table 7.** Specifications for instrumented mouthguards used in this study.

	In-mouth (ADXL377/ L3G4200D)	Stanford MiG2.0	Prevent iMG	HITIQ Nexus	Wake Forest Mouthpiece
Sampling rate (Accel)	1024 Hz	1000 Hz	3200 Hz	3200 Hz	350 <sup>a</sup> , 4684 <sup>b</sup> , & 6400 <sup>c</sup> Hz
Sampling rate (Gyro)	1024 Hz	8000 Hz	3200 Hz	800 Hz	350 <sup>a</sup> , 1565 <sup>b</sup> , & 6400 <sup>c</sup> Hz
Measurement range (Accel)	± 200 g (1 tri-axis)	± 400 g (1 tri-axis)	± 200 g (1 tri-axis)	± 200 g (3 tri-axis)	± 200g (1 tri-axis)
Measurement range (Gyro)	± 40 rad/s (1 tri-axis)	± 70 rad/s (1 tri-axis)	± 35 rad/s (1 tri-axis)	± 35 rad/s (1 tri-axis)	± 35 <sup>a,c</sup> rad/s ± 40 <sup>b</sup> rad/s (1 tri-axis)
Output time window	100 [-25, 75] ms	200 [-49, 150] ms	50 [0, 50] ms	100 [-20, 80] ms	60 [-15, 45] ms
Triggering sensor	Accel.	Accel.	Accel.	Accel.	Accel.
Triggering threshold	10 G	10 G	5 G	8 G	5 G
No. measured impacts	1	771	2280	795	5

*a: Gymnastics, b: ice hockey, c: American football*

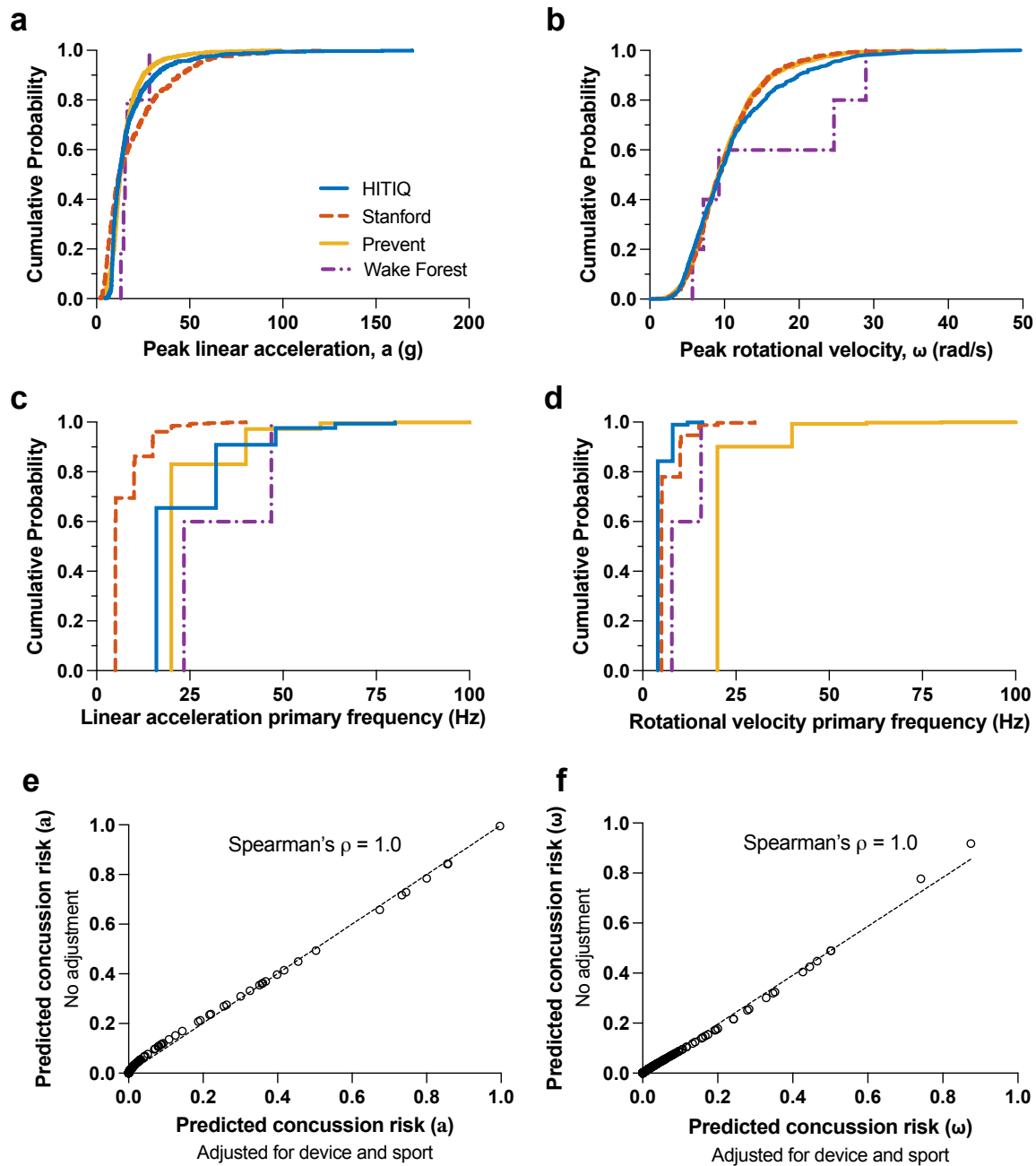
**Extended Data Table 8.** Results of Kolmogorov-Smirnov test to compare the distributions of measured kinematics between mouthguard devices. Distributions for measured  $a$  (g),  $\omega$  (rad/s), and their primary frequencies (Hz) were compared.

Mouthguard 1	Mouthguard 2	P value			
		$a$ (g)	$a$ (Hz)	$\omega$ (rad/s)	$\omega$ (Hz)
HITIQ	Stanford	$3.42 \times 10^{-23}$	$1.33 \times 10^{-318}$	0.020	$2.45 \times 10^{-245}$
HITIQ	Prevent	$9.78 \times 10^{-6}$	$8.39 \times 10^{-223}$	0.002	0
HITIQ	Wake Forest	0.00713	0.00144	0.464	$5.61 \times 10^{-4}$
Stanford	Prevent	$1.48 \times 10^{-18}$	0	0.922	0
Stanford	Wake Forest	0.00940	$2.80 \times 10^{-5}$	0.359	$1.85 \times 10^{-3}$
Prevent	Wake Forest	0.00905	$7.01 \times 10^{-4}$	0.374	$1.93 \times 10^{-5}$

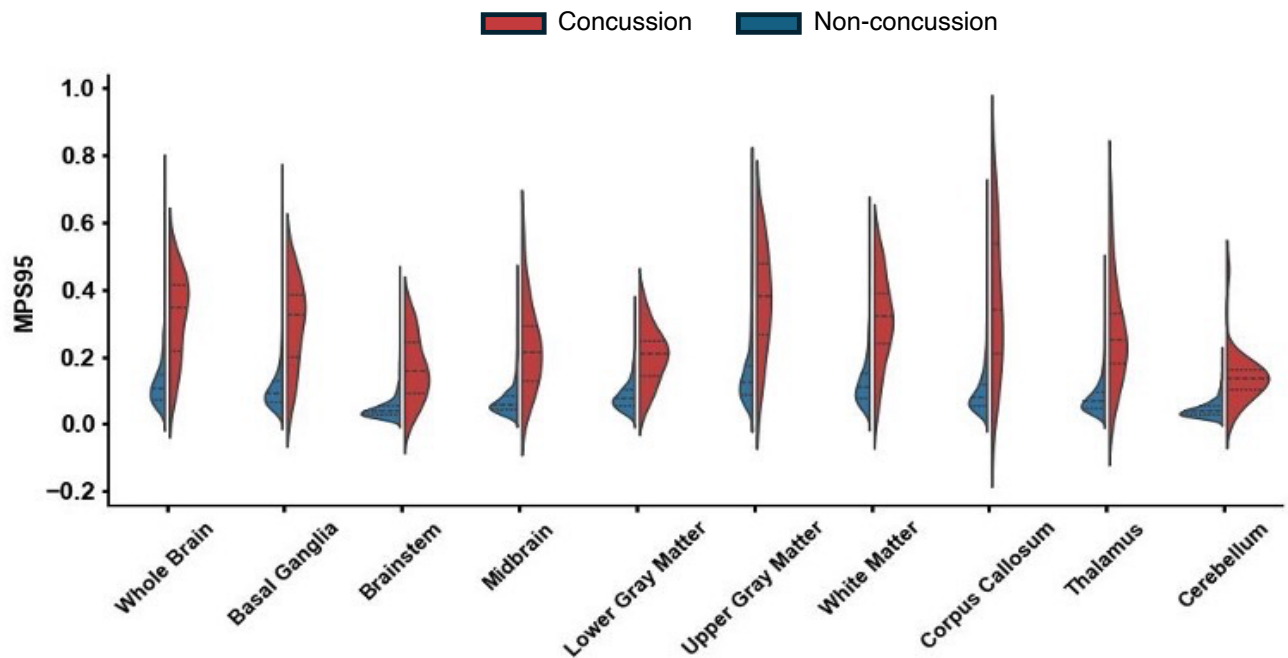
**Extended Data Table 9.** Results from LASSO-penalized logistic regression and dominance analysis for unique predictors screened for injury risk function development.

Predictor	General Dominance (McFadden $R^2$ )	LASSO Coefficient (standardized)
$a$	0.108	0.912
$\omega$	0.065	0.842
$\alpha$	0.061	0.380
HIC36	0.051	-0.097
MPS95	0.050	0.206
HIP <sub>rot</sub>	0.046	-0.005
BrIC	0.046	-0.362
HIP	0.042	0.000
HIP <sub>lin</sub>	0.041	0.000
CP	0.029	-0.242





**Extended Data Figure 1.** Empirical cumulative distribution functions comparing peak kinematic measurements in the time and frequency domains across datasets with different mouthguard devices. **a**, Peak linear acceleration and **b**, peak rotational velocity distributions for each iMG. Distribution of primary frequencies for **c**, peak linear acceleration and **d**, peak rotational velocity. We note that HITIQ data reflect raw signals reprocessed using a 200 Hz low-pass filter, not the manufacturer's default output. **e-f**, Comparison of concussion risk predicted with and without adjusting the logistic regression model for mouthguard device type and sport using **e**, peak linear acceleration and **f**, peak rotational velocity. Despite measurable differences in kinematic distributions across mouthguard devices, adjusting for device and sport had minimal influence on predicted risk.



**Extended Data Figure 2.** Distribution of regional MPS95. Points are plotted per-player per-region. Dashed lines represent the median and interquartile range

## Extended Data References

1. Domel, A. G. *et al.* A new open-access platform for measuring and sharing mTBI data. *Sci Rep* **11**, 7501 (2021).
2. Hernandez, F. *et al.* Six Degree-of-Freedom Measurements of Human Mild Traumatic Brain Injury. *Ann Biomed Eng* **43**, 1918–1934 (2015).
3. Bartsch, A. J. *et al.* High Energy Side and Rear American Football Head Impacts Cause Obvious Performance Decrement on Video. *Ann Biomed Eng* **48**, 2667–2677 (2020).
4. Tiernan, S. *et al.* Concussion and the severity of head impacts in mixed martial arts. *Proc Inst Mech Eng H* **234**, 1472–1483 (2020).
5. Evans, L. J. *et al.* Associations Between Instrumented Mouthguard-Measured Head Acceleration Events and Post-Match Biomarkers of Astroglial and Axonal Injury in Male Amateur Australian Football Players. *Sports Med* (2024) doi:10.1007/s40279-024-02138-6.
6. Pritchard, N. S., E. Urban, J., Miller, L. E., Lintner, L. & Stitzel, J. D. AN ANALYSIS OF HEAD KINEMATICS IN WOMEN'S ARTISTIC GYMNASTICS. *SGJ* **12**, 229–242 (2020).
7. Swenson, A., Miller, L., Urban, J. & Stitzel, J. Head Kinematics by Contact Scenarios in Youth Ice Hockey. *Neurology* **95**, (2020).
8. Newman, J. A. Head Injury Criteria in Automotive Crash Testing. in 801317 (1980). doi:10.4271/801317.
9. Takhounts, E. G., Craig, M. J., Moorhouse, K., McFadden, J. & Hasija, V. Development of Brain Injury Criteria (BrIC). in 2013-22-0010 (2013). doi:10.4271/2013-22-0010.
10. Rowson, S. & Duma, S. M. Brain Injury Prediction: Assessing the Combined Probability of Concussion Using Linear and Rotational Head Acceleration. *Ann Biomed Eng* **41**, 873–882 (2013).
11. Newman, J. A. & Shewchenko, N. A Proposed New Biomechanical Head Injury Assessment Function - the Maximum Power Index. in 2000-01-SC16 (2000). doi:10.4271/2000-01-SC16.
12. Gabler, L. F., Crandall, J. R. & Panzer, M. B. Development of a Second-Order System for Rapid Estimation of Maximum Brain Strain. *Ann Biomed Eng* **47**, 1971–1981 (2019).
13. Gabler, L. F., Joodaki, H., Crandall, J. R. & Panzer, M. B. Development of a Single-Degree-of-Freedom Mechanical Model for Predicting Strain-Based Brain Injury Responses. *Journal of Biomechanical Engineering* **140**, 031002 (2018).

## Supplementary Information

### Comparison of mouthguard measurement devices

To assess measurement consistency across iMGs after 200 Hz filtering, we computed empirical cumulative distribution functions of peak linear acceleration ( $a$ ), peak rotational velocity ( $\omega$ ), and their primary frequencies for impacts recorded by each iMG (Extended Data Figure 1). These metrics were chosen because they are directly measured by the accelerometer(s) and gyroscope contained on each iMG sensor board. To characterize the primary frequency, we first computed the resultant of the triaxial measurements for linear acceleration and rotational velocity using the Euclidean norm. Each resultant trace was demeaned to remove any DC offset. To extract the primary frequency, we computed the discrete Fourier transform (`fft` in MATLAB) of each demeaned signal to obtain the single-sided amplitude spectrum. The frequency bin with the largest magnitude, excluding the zero-Hz component, was recorded as the primary frequency and used to construct cumulative distribution functions (Extended Data Figure 1c-d). In parallel, we extracted the peak values of the resultant  $a$  and  $\omega$  time traces and plotted their cumulative distribution functions (Extended Data Figure 1a-b).

To quantitatively assess whether the distributions differed significantly across iMGs, we performed pairwise two-sample Kolmogorov–Smirnov (KS) tests for each metric. These revealed statistically significant differences ( $p < 0.05$ ) in both time- and frequency-domain metrics between several device pairs (Extended Data Table 8). While KS tests can detect differences in measurement distributions, they do not necessarily indicate that these differences meaningfully alter injury risk predictions. To evaluate this, we constructed additional Bayesian univariate logistic regression models for  $a$  and  $\omega$ , including random intercepts for mouthguard type and sport, as well as an offset to account for the rare incidence of concussion (5.5 concussions per 1000 impacts).<sup>1</sup> We compared predicted concussion probabilities from this model to those from our main model that did not include random effects. The correlation between predicted risks from the two models was extremely high across all predictors (Extended Data Figure 1), suggesting that despite distributional differences between devices, the influence on estimated concussion risk was negligible.

### Brain sensitivity to rotational velocity and acceleration

To evaluate whether brain strains in our dataset were more sensitive to peak rotational velocity ( $\omega$ ) or peak rotational acceleration ( $\alpha$ ), we plotted the 95<sup>th</sup> percentile maximum principal strain from the DAMAGE<sup>2</sup> model as a function of both  $\omega$  and  $\alpha$  and examined where human impacts fell relative to a fixed slope representing the brain's

natural frequency (Extended Data Figure 3). First, we defined a two-dimensional grid of peak rotational velocities ( $\omega$ : 0.1–100 rad/s) and peak rotational accelerations ( $\alpha$ : 1–20,000 rad/s<sup>2</sup>) spanning the full range of head impacts in our dataset. For each ( $\omega$ ,  $\alpha$ ) pair, a half-sine rotational-acceleration pulse was constructed at 1 ms resolution over a 2 s window, and used as input to the DAMAGE model. The resulting triplets [ $\omega$ ,  $\alpha$ , DAMAGE] formed a simulation-only design matrix. To create continuous contour surfaces, these discrete DAMAGE values were interpolated onto the ( $\omega$ ,  $\alpha$ ) mesh using MATLAB's `griddata` function with a natural neighbor scheme. Next, we computed DAMAGE for the 3,852 human impacts in our dataset and overlaid them on the interpolated contours. Finally, to demarcate the kinematic boundary where  $\omega$  and  $\alpha$  contributions to brain strain are equal, we overlaid a straight reference line whose slope is directly proportional to the brain's natural frequency ( $f_n$ ) using Equation 1,

$$\alpha = \pi f_n \omega \quad (1)$$

where  $f_n$  was estimated to be 25.1 Hz across the coronal, axial, and horizontal anatomical planes.<sup>3</sup>

### Candidate models for classification and injury risk function development

We evaluated twelve logistic regression models to compare the predictive value of linear, rotational, and strain-based metrics for concussion classification and injury risk modeling. These models were selected based on their prevalence in head injury biomechanics research and safety standards. To prioritize which models were included in injury risk function development and comparative statistical testing, we applied multiple screening approaches including deviance, Bayesian Information Criterion, LASSO-penalized logistic regression, and dominance analysis.

Deviance and Bayesian Information Criterion assessed model fit across the twelve candidates. LASSO and dominance analysis were conducted using the ten unique predictors represented in these models (Extended Data Table 9). LASSO was performed using the `glmnet` R package with a binomial family and 5-fold cross-validation to identify the optimal penalty parameter, lambda. The L1 regularization penalty constrains the sum of the absolute values of the coefficients (n=10 coefficients) to be less than or equal to the specified constant determined by lambda, encouraging sparsity. Predictors were standardized prior to fitting. Dominance analysis was conducted on a full logistic regression model (n=10 predictors) using the `dominanceanalysis` R package. General dominance scores were computed using McFadden's pseudo-R<sup>2</sup> to quantify each predictor's average contribution across all possible subset models.

LASSO and dominance analysis also complemented our other statistical approaches. Specifically, odds ratios quantified the direction and strength of each predictor's independent association with injury risk; area under the precision-recall curve measured the classification performance of each model in the context of class imbalance;

LASSO identified relative predictor importance under regularized logistic regression; and dominance analysis estimated each predictor's average contribution to model fit. Across these approaches,  $a$ , followed by  $\omega$  and  $\alpha$  consistently ranked among the most important and best-fitting predictor variables. As a result, we focused injury risk function development on models containing these three predictors. This prioritization ensured that the resulting injury risk functions were both well-fitting and practically useful, and reduced the number of formal statistical comparisons needed, thereby preserving statistical power on our limited concussion dataset. Other potential predictors, such as region-specific brain strains or directional kinematics, were excluded due to limited sample size of the concussions. We also excluded peak linear velocity, as it is not a widely used injury metric in safety standards or head injury research.

## References for Supplementary Information

1. Rowson, S. & Duma, S. M. Brain Injury Prediction: Assessing the Combined Probability of Concussion Using Linear and Rotational Head Acceleration. *Ann Biomed Eng* **41**, 873–882 (2013).
2. Gabler, L. F., Crandall, J. R. & Panzer, M. B. Development of a Second-Order System for Rapid Estimation of Maximum Brain Strain. *Ann Biomed Eng* **47**, 1971–1981 (2019).
3. Gabler, L. F., Joodaki, H., Crandall, J. R. & Panzer, M. B. Development of a Single-Degree-of-Freedom Mechanical Model for Predicting Strain-Based Brain Injury Responses. *Journal of Biomechanical Engineering* **140**, 031002 (2018).